Beyond equilibrium: Multi-method mass-balance monitoring at the vanishing Alpine glacier Stubacher Sonnblickkees, Austria

Journal:	*Journal of Glaciology*
Manuscript ID	Draft
Manuscript Type:	Article
Date Submitted by the Author:	n/a
Complete List of Authors:	Siebenbrunner, Anna; Technical University of Munich, Chair of Landslide Research; Georesearch Research Company, Zagel, Bernhard; Paris Lodron University of Salzburg Department of Geoinformatics – Z_GIS Gschwentner, Andreas; Austrian Academy of Sciences, Institute for Interdisciplinary Mountain Research Delleske, Robert; Georesearch Research Company, Sonnleitner, Amelie; Georesearch Forschungsgesellschaft mbH; University of Salzburg, Department of Environment and Biodiversity Wiesenegger, Hans; Hydrological Service of Land Salzburg Hartl, Lea; Austrian Academy of Sciences, Institute for interdisciplinary mountain research
Keywords:	Glacier mass balance, Glacier monitoring, Remote sensing
Abstract:	Glaciers in the Eastern Alps are approaching extinction, raising the question of how reliably established mass-balance monitoring methods perform on glaciers in severe disequilibrium. We present a multi-year (2018–2025) intercomparison of three independent methods – direct glaciological, semi-direct (accumulation-area-ratio based) and UAV-geodetic – at Stubacher Sonnblickkees (SSK), Austria, complemented by geodetic–(semi-)direct comparisons over two historical periods (1969–1998, 2008–2023). After homogenisation onto a common area time series, no method pair differs significantly at the 95 % level during the

	intercomparison period. The mean annual deviation of 0.1 m w.e./a between the direct and geodetic methods is among the lowest reported in comparable studies. Cumulative annual UAV-geodetic mass balances agree with 2018–2025 DEM differencing to within 0.25 m w.e., demonstrating that annual high-resolution surveys capture multi-year change without systematic drift. While these multi-year comparisons indicate good overall alignment, the annual comparison reveals substantial year-to-year deviations between methods that warrant further investigation. Since 2022, accelerating disintegration exposes method-specific limits, most critically the breakdown of the semi-direct method as the accumulation area vanishes. Sustaining adaptive, multi-method monitoring is essential to preserve long-term mass-balance records as these glaciers vanish, and to extend them onto larger successor glaciers.

Journal of Glaciology, Vol. 00, No. 0, 0000

Beyond equilibrium: Multi-method mass-balance monitoring at the vanishing Alpine glacier Stubacher Sonnblickkees, Austria

Anna SIEBENBRUNNER[1,2]*, Bernhard ZAGEL[3], Andreas GSCHWENTNER[4], Robert DELLESKE[2], Amelie SONNLEITNER[2,5], Hans WIESENEGGER[6], Lea HARTL[4]

[1] *Technical University of Munich, Chair of Landslide Research, Munich, Germany*

[2] *GEORESEARCH Forschungsgesellschaft mbH, Puch bei Hallein, Austria*

[3] *University of Salzburg, Department of Geoinformatics - Z_GIS, Salzburg, Austria*

[4] *Austrian Academy of Sciences, Institute for Interdisciplinary Mountain Research, Innsbruck, Austria*

[5] *University of Salzburg, Department of Environment and Biodiversity, University of Salzburg, Austria*

[6] *Hydrological Service of Land Salzburg (retired)*

Correspondence: Anna Siebenbrunner <anna.siebenbrunner@tum.de>

ABSTRACT. Glaciers in the Eastern Alps are approaching extinction, raising the question of how reliably established mass-balance monitoring methods perform on glaciers in severe disequilibrium. We present a multi-year (2018–2025) intercomparison of three independent methods – direct glaciological, semi-direct (accumulation-area-ratio based) and UAV-geodetic – at Stubacher Sonnblickkees (SSK), Austria, complemented by geodetic–(semi-)direct comparisons over two historical periods (1969–1998, 2008–2023). After homogenisation onto a common area time series, no method pair differs significantly at the 95 % level during the intercomparison period. The mean annual deviation of 0.1 m w.e. a^{-1} between the direct and geodetic methods is among the lowest reported in comparable studies. Cumulative annual UAV-geodetic mass balances agree with 2018–2025 DEM differencing to within 0.25 m w.e., demonstrating that annual high-resolution surveys capture multi-year change without systematic drift. While these multi-year comparisons indicate good

*Present address: Chair of Landslide Research, Technical University of Munich, Arcisstraße 21, 80333 Munich, Germany.

overall alignment, the annual comparison reveals substantial year-to-year deviations between methods that warrant further investigation. Since 2022, accelerating disintegration exposes method-specific limits, most critically the breakdown of the semi-direct method as the accumulation area vanishes. Sustaining adaptive, multi-method monitoring is essential to preserve long-term mass-balance records as these glaciers vanish, and to extend them onto larger successor glaciers.

1 INTRODUCTION

Glaciers in the Eastern Alps are projected to largely disappear by the end of the century (Van Tricht and others, 2025), with smaller Austrian glaciers likely reaching this threshold even sooner (Hartl and others, 2025b). This trend of accelerated mass loss is already well-documented (Hugonnet and others, 2021; Zemp and others, 2025), characterized by rapid thinning, increased subglacial melt, and fundamental shifts in physical properties that ultimately lead to glacial collapse (Hugonnet and others, 2021; Hösli and others, 2025).

This rapid transition into a state of extreme disequilibrium raises a critical methodological question: are conventional mass-balance monitoring techniques – originally developed for balanced or accumulating glaciers – still robust under present-day climate conditions? As glaciers fragment and thin, the assumptions underlying conventional surface-based mass-balance methods are increasingly strained, raising the question of whether independent methods still converge on a consistent mass-loss signal under such conditions (Huss and others, 2012; Carturan and others, 2020; Huss and others, 2021).

Historically, glacier mass balance (MB) was determined annually via the direct glaciological method, often supplemented by hydrological observations. More recently, automated camera-based systems for near-real-time stake readings are increasingly being deployed to augment traditional ablation stake networks (Landmann and others, 2021). The emergence of geodetic techniques enabled the first systematic intercomparison with glaciological MB data (Funk and others, 1997; Andreassen, 1999). While early reanalyses relied on terrestrial and aerial photogrammetry (Zemp and others, 2010; Fischer, 2011), more recent work has also utilised elevation change information derived from multi-temporal laser scanning (Klug and others, 2018). Furthermore, the integration of Unoccupied Aerial Vehicle (UAV) photogrammetry has introduced

high-resolution geodetic surveys to bridge the gap between point measurements and glacier-wide scales (Geissler and others, 2021; Van Tricht and others, 2021). Together, these advancements are shifting monitoring efforts toward broader spatial coverage and higher temporal resolution. However, comparability across methods and studies remains an open challenge: Hock and others (2026) recently identified four systematic obstacles – inconsistent reporting, differences in the mass-balance components included, differences in time span, and differences in spatial domain – that hinder the synthesis of published estimates and called for more rigorous reporting and open-data practices.

In addition, every monitoring method carries inherent biases, and the "true" mass balance remains an elusive target (Hock and others, 2026). It is scientifically reasonable to consider different methods to agree when their long-term results converge within method-specific uncertainty bounds. Evaluating the inter-method agreement of these monitoring approaches is therefore essential, as mass-balance data serve as the primary input data for glacier evolution models, which in turn underpin projections of future glacier change and its downstream impacts on water resources, hydropower generation, ecosystem dynamics, as well as sea-level rise and related hazards (Huss and Hock, 2018; Hock and others, 2019, 2022). There is a critical need to ensure the continuity and "rescue" of long-term mass-balance series, particularly as the glaciers providing these records face extinction (Geibel and others, 2022). Preserving these datasets through the transition to new monitoring technologies constitutes a key research priority.

This context highlights the value of glaciers with long-term, multi-method monitoring records (Huss and others, 2025). One such site is Stubacher Sonnblickkees (SSK) in the Hohe Tauern range, Austria (Slupetzky and others, 2014). Systematic glaciological observations at SSK began in 1963, with mass-balance estimates reconstructed back to 1949 (see subsection 2.2), making it one of the longest-running glacier observation sites in Austria. Between 2018 and 2025, three independent methods were applied in parallel at SSK: the direct glaciological method, a semi-direct method based on the Accumulation Area Ratio (AAR), and UAV-borne photogrammetry to derive geodetic mass balance. SSK has already begun to disintegrate and is expected to vanish entirely by the 2030s.

The combination of (i) a robust historical record of (semi-) direct mass-balance observations, (ii) the availability of additional geodetic mass-balance data, (iii) the simultaneous application of three independent methods (including novel high-resolution UAV surveys) for multiple years, and (iv) the glacier's imminent disappearance makes SSK an ideal case study. This paper addresses the preservation of long-term mass-balance records in the face of glacier extinction and evaluates the specific methodological challenges arising

from rapid disintegration in recent years.

2 DATA AND METHODS

2.1 Study site

Stubacher Sonnblickkees is a small slope-type glacier located in the Hohe Tauern Range of the Eastern Alps, within the Province of Salzburg, Austria (47.12 ° N, 12.67 ° E). The east-facing glacier lies along the main Alpine crest in the Upper Stubach Valley, and spanned elevations from approximately 3,050 m to 2,500 m a.s.l. in the 1980s, nowadays ranging from 3,050 m to 2,650 m. Its area decreased from 1.7 km^2 in the early 1980s to around 0.6 km^2 by 2025. The glacier's irregular topography (see Figure 1), shaped by complex subglacial terrain, results in highly variable accumulation and ablation conditions, with pronounced effects from wind redistribution and spatially heterogeneous snow deposition (Slupetzky, 2015).

SSK was selected as a long-term monitoring site due to its topographic complexity, proximity to Rudolfshütte (formerly operated by the Austrian Alpine Club), and access to hydrometeorological infrastructure (Slupetzky, 2015). The monitoring programme at SSK continues to contribute to glacier-climate studies in the Eastern Alps and supports broader assessments of high-mountain hydrology and climate change impacts within the European long-term ecosystem research framework (eLTER) (Zagel and others, 2024).

2.2 Mass-balance monitoring at Stubacher Sonnblickkees

Between 1963 and 1981, annual mass balance was determined through direct measurements (hereafter referred to as calibration period), including extensive networks of ablation stakes and snow pits. From 1981 onward, a regression-based approach was developed using the Accumulation Area Ratio (AAR) (hereafter referred to as semi-direct method (Slupetzky, 1989)). The initial aim was to extend the record back in time, with photographic reconstructions of AAR allowing extrapolation back to 1949 (Günther and Widlewski, 1986; Slupetzky, 2015). The mass-balance time series of semi-direct measurements was then maintained under the International Hydrological Decade (1965–1974), the International Hydrological Programme (1975–1981), and subsequently by the Hydrological Service of Land Salzburg. Research activities were led by the University of Salzburg, particularly from the Department of Geography and the High Alpine Research Station (1982–1999) (Slupetzky and others, 2014). A mass balance measurement programme using the direct glaciological method was reinstated in 2017 by the Hydrological Service of Land Salzburg and implemented by the Institute for Interdisciplinary Mountain Research of the Austrian

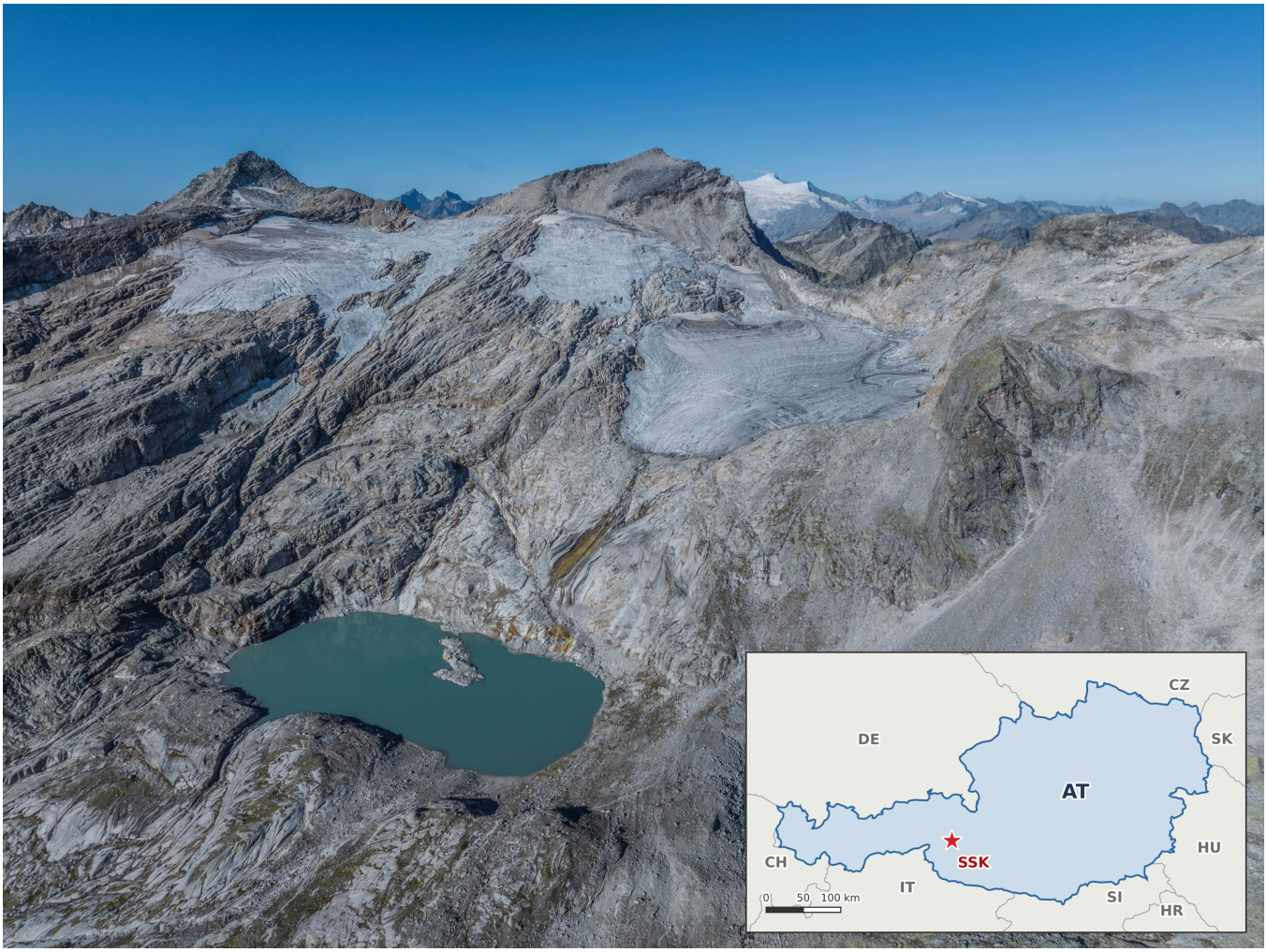

Fig. 1. The rapidly disintegrating Stubacher Sonnblickkees and its surrounding area. The lake "Unterer Eisbodensee" emerged in the 1980s and was partly covered by ice until 2017 (photo: GEORESEARCH, 2025). The map shows the location of the study site within Austria (AT).

Academy of Sciences. Direct measurements are available from 2018 through 2025. In addition, starting in 2018, annual UAV-based photogrammetry campaigns to monitor geodetic mass balance were carried out by GEORESEARCH, a non-university, non-profit research institute based in Salzburg. The purpose of this multi-method monitoring initiative was to allow for comparative analyses and to evaluate agreement among methods over multiple years.

The resulting long-term mass-balance series, highlighting both the 1964–1980 calibration period and the intensified multi-method monitoring in the most recent years, is presented in Figure 2.

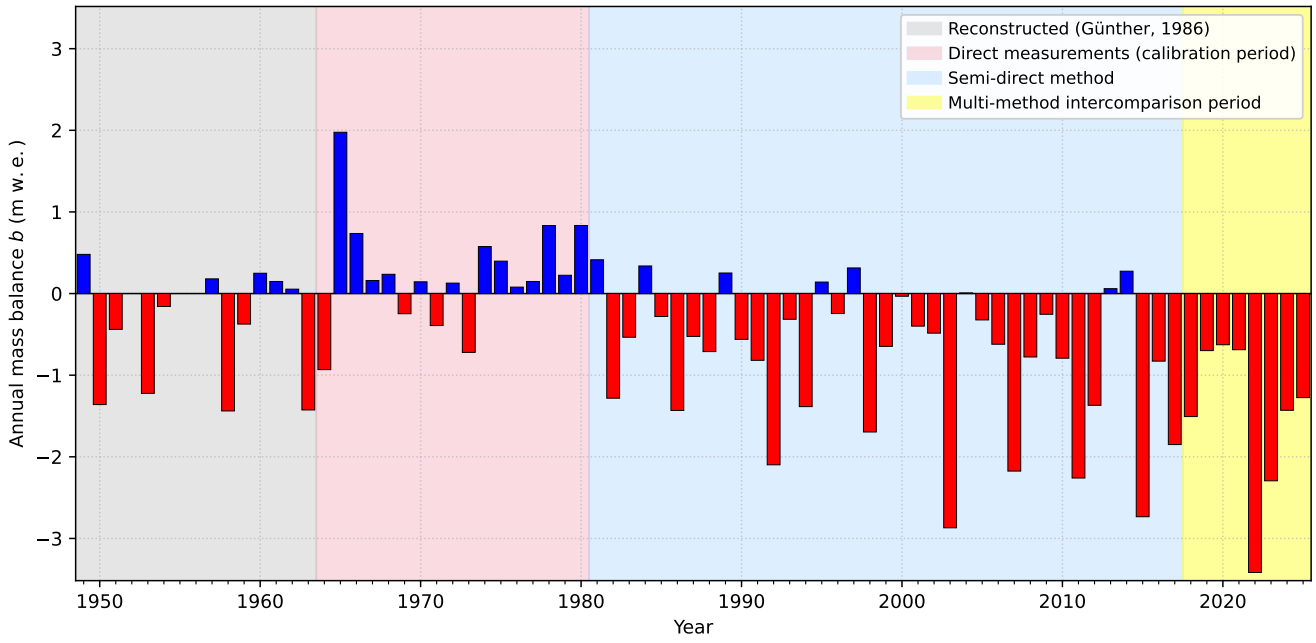

Fig. 2. Time series of annual mass balance (b) for the period 1964–2025 as published in World Glacier Monitoring Service (2026). Background shading indicates periods of different methodological approaches, including (i) data reconstruction by Günther and Widlewski (1986) (grey), (ii) the initial period of direct measurements (red), (ii) the subsequent single-method period relying on semi-direct measurements only (blue), and (iv) the current multi-method monitoring period (yellow), which is the primary focus of this analysis. MB values plotted for period (iv) are unhomogenised data derived from the semi-direct method.

All three methods considered for this study's mass-balance intercomparison exercise are described in detail in the following. Representative images illustrating the applied methodologies are shown in Figure 3.

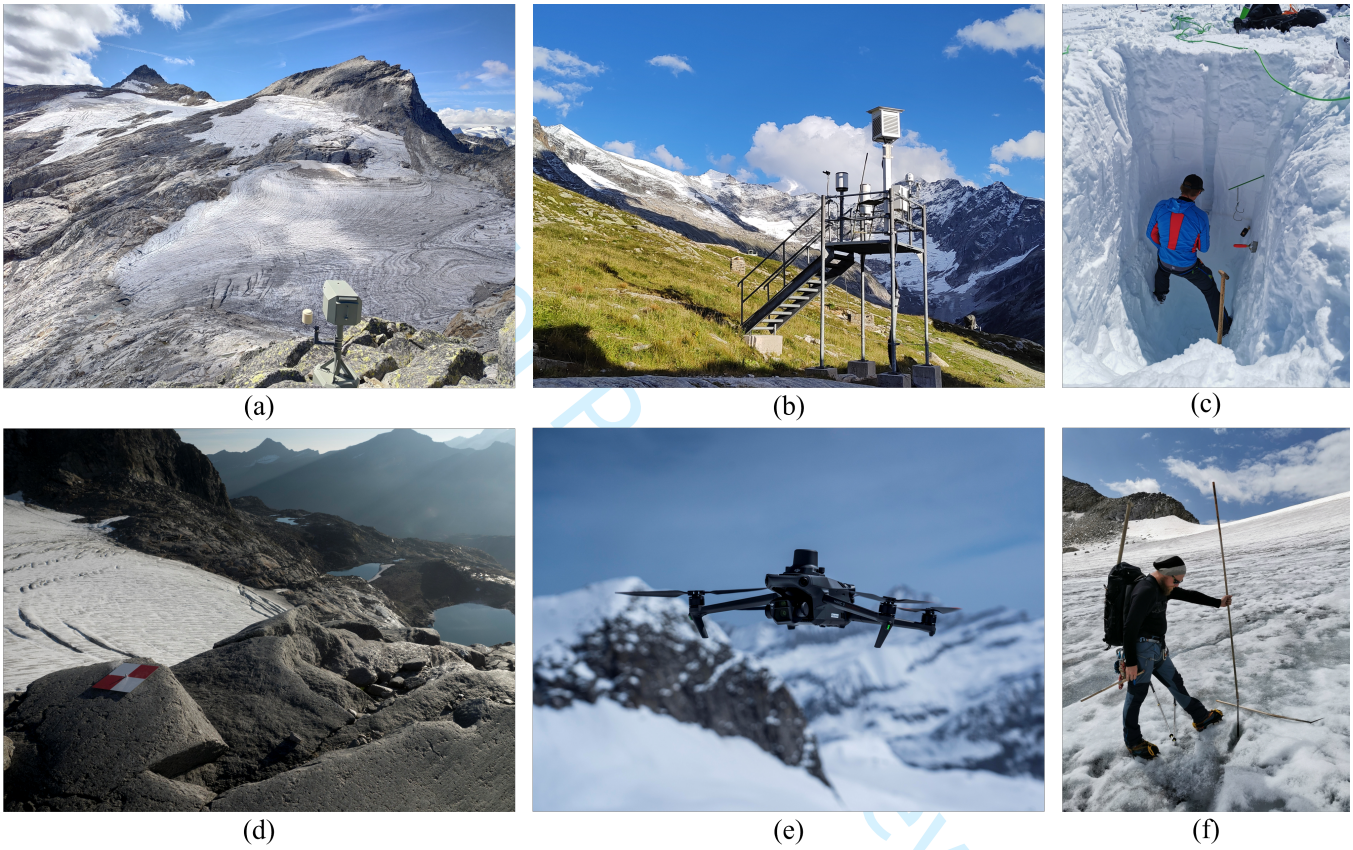

Fig. 3. Technical monitoring infrastructure at SSK: (a) stationary single-lens reflex (SLR) camera at Hochfürlegpfeiler (since 2012); (b) weather station "Rudolfshütte", operated by GeoSphere Austria since 1992; (c) snow pit; (d) ground control point (GCP) for UAV-borne geodetic mass balance (installed in 2018); (e) UAV employed for geodetic mass balance; (f) ablation stake (photos: (a) BZ, 2025; (b) BZ, 2023; (c) AG, 2021; (d) RD, 2018; (e) RD, 2024; (f) AG, 2021)

.

2.2.1 Direct glaciological method

The surface mass balance of SSK is monitored using the direct glaciological method, a standard approach in Alpine glacier studies that has been applied in mass balance monitoring programmes in Austria for several decades (e.g., Hoinkes, 1970; Cogley and others, 2011; Fischer and others, 2015; Hartl and others, 2024). This method quantifies seasonal accumulation and ablation based on point-scale field observations (i.e., snow pits, ablation stakes) and extrapolates them to the entire glacier area.

For specifics related to the first period of direct measurements (1964–1980, Figure 2), we refer to Slupetzky (2015) and references therein. To reinstate direct glaciological measurements for the current method intercomparison, a new network of 13 ablation stakes was installed during the 2017 summer season and snow pit locations were selected in the upper parts of the glacier. The 2018 hydrological year was the first complete year in the new time series. In the following years, some stake positions were adjusted to account for rapid area losses in the lower sections of the glacier. Stakes were typically drilled to about 8 m depth using a steam drill and periodically redrilled to prevent melt-out. The total number of ablation stakes used per season ranged from a maximum of 15 (2023, 2024) to 10 (2025).

Stake readings were recorded at intervals of about 3–4 weeks throughout the ablation seasons, with a final survey as close as possible to the end of the hydrological year (September 30). Ice loss was computed from the difference in exposed stake length between visits and converted to water equivalent (w. e.) using an ice density ρ_{ice} of 900 kg m^{-3}. Up to the 2022 mass balance season, mass change in the accumulation zone was determined by density measurements at a snow pit and snow depth probing. Snow depths at the measurement points were converted to water equivalent values using the bulk density measured in the snow pit. After 2022, annual mass balance was determined from the stake readings only because no seasonal snow or firn remained at the end of the ablation season.

The point-scale data from the final annual survey were extrapolated in time to the end of the hydrological year (September 30) by estimating melt and/or snow water equivalent based on the most recently observed melt rates and meteorological data. That is, the current direct glaciological measurement program uses a fixed-date system (e.g., Cogley and others, 2011). Figure A1 shows the dates of the final surveys compared to the end of the hydrological year. The surveys occurred within 10 days of the fixed date in all years.

In addition to annual mass balance, winter mass balance was determined via dedicated campaigns around the end of the accumulation season, as close as possible to April 30. Seasonal snow depth and

bulk density were determined at one to two snow pits, and extensive snow depth probing was carried out to assess snow distribution across the glacier. As above, snow depths and density measurements were combined to compute water equivalent values of mass balance at the measurement points.

All field measurements were georeferenced using GPS or differential GPS. The point measurements of winter and annual mass balance were extrapolated to the glacier area by manually drawing contour lines of equal mass balance in water equivalent values (e.g., Østrem and others, 1991). Contour intervals were set to 0.5 m w.e. in the ablation zone and 0.25 m w.e. in the accumulation zone. The area of the accumulation zone (S_c) in a given year is defined as the area of positive mass change (if any) delineated by the zero mass balance contour. Conversely, the ablation area (S_a) is the area of negative mass balance.

Mass balance values as obtained with the contour line approach were integrated over the glacier area and over different elevation bands to determine the glacier-wide mass balance (B) and values per elevation zone, as described in, e.g., Hartl and others (2024) for other mass balance monitoring sites in the region. The specific mass balance ($\overline{b}$) was derived as:

$$\overline{b} = \frac{B}{S}, \tag{1}$$

where S is the total glacier area.

During initial processing of the direct glaciological data set, the most recent available glacier outlines for a given year (typically an outline of the previous summer mapped from satellite imagery or orthophotos), and a digital elevation model acquired in 2008 were used to determine glacier-wide mass balance and elevation zone values (Gschwentner and others, 2026). For the study at hand, the data were reprocessed to homogenize glacier area for the method intercomparison using outlines and topographic information derived from annual UAV-based photogrammetric surveying (see following sections). Annual $\overline{b}$ was determined using the average of the glacier area S_t of the previous summer and the area of the current (S_{t+1}) summer (Florentine and others, 2023).

For this study, we assume an uncertainty in b of $\sigma_b = \pm 340$ mm w. e. a^{-1} based on average uncertainty values for glacier-wide direct mass balance given in Zemp and others (2013). Quantitative evaluations of all components of the error equation associated with b (all possible sources of type A and B uncertainties) are challenging to obtain and uncertainty estimates are typically derived from point-scale uncertainties or comparisons with independent data, such as multi-year geodetic mass balance. Due to the relatively dense stake network and very limited accumulation in recent years at SSK, we assume that the above value is a

relatively conservative uncertainty estimate for b during the 2018–2025 intercomparison period, and that it encompasses uncertainties related to extrapolation in space (drawing of contour lines) and time (floating to fixed-date), as well as uncertainties in the point measurements.

2.2.2 Semi-direct method

Based on the direct mass balance measurements from 1964 to 1980 (Figure 2), Slupetzky (1989) established regression equations relating the annual mean specific mass balance (b) to the Accumulation Area Ratio (AAR). The AAR is defined as the ratio of the accumulation area (S_c) to the total glacier area (S). Direct measurements were discontinued after 1980 due to financial constraints, prompting the use of these equations to calculate mass balance semi-directly. The critical prerequisite for this method is accurately determining S_c at the end of each balance year, which was achieved by mapping the minimum snow cover extent.

The specific net accumulation ($b_c = B_c/S$) and specific net ablation ($b_a = B_a/S$) are mathematically described as follows (Slupetzky, 2015):

$$b_c = 29.19 \cdot \left[-\ln\left(1 - \frac{S_c}{S}\right)\right]^{1.125} \quad , \tag{2}$$

$$b_a = 56.808 \cdot \ln\left(\frac{S_c}{S}\right) - 0.925 \quad . \tag{3}$$

The net specific mass balance b is consequently obtained as:

$$b = b_c + b_a \quad . \tag{4}$$

These equations account for the non-linear relationship between AAR and b, ensuring that the mass-balance factor (AAR) approaches 1.0 when the entire glacier constitutes the accumulation area, and 0 when it is entirely an ablation area. For SSK, a balanced budget ($b = 0$) corresponds to an AAR factor of 0.62 (Slupetzky, 2015).

To quantify the uncertainty of the semi-direct method, Slupetzky and others (2014) combined static and dynamic uncertainty factors. Their static uncertainty factor stems from a reanalysis study conducted by Fischer (2011), which compared the cumulative semi-direct mass balances with mass changes geodetically derived from digital elevation models for 1969 and 1998 (Kuhn and others, 2015; Patzelt, 2015). This

comparison yielded an average annual deviation of 0.16 m w. e. for the semi-direct mass balance. To represent the AAR-related uncertainty, primarily governed by the ratio S_c/S, an additional heuristic term σ_{AAR} (personal communication from B. Zagel, 2026) is applied:

$$\sigma_{AAR} = \frac{1}{AAR} \cdot \frac{1}{1000} \quad . \tag{5}$$

This term is not derived from a formal error budget; it is included to reflect the expectation that uncertainty increases as the accumulation area shrinks, by assigning a larger penalty to very small AAR values.

Hence, the estimated total yearly uncertainty of the semi-direct method σ_{semi} is $0.16 + \sigma_{AAR}$ m w.e.

Inherent to the formula used to calculate b_a, the semi-direct method is no longer applicable once there is no accumulation area left ($S_c = 0$). This leads to $\ln\left(\frac{S_c}{S}\right) = \ln(0)$, which is undefined in the real number system. If the entire glacier area became an accumulation area (AAR = 1), the mathematical limits of this method would also be reached (see Equation 2).

2.2.3 Geodetic mass balance

UAV-borne photogrammetry was used to derive high-resolution surface elevation data of SSK for geodetic mass-balance analysis. The general principles of structure-from-motion (SfM) and multi-view stereo (MVS) photogrammetry follow well-established approaches (e.g., Westoby and others, 2012). Throughout this study, we use the term "geodetic" in the conventional glaciological sense of surface-elevation differencing, following Cogley and others (2011); we note that Hock and others (2026) caution against its unqualified use, as in geodesy proper the term also encompasses gravimetric approaches.

The mass-balance calculations of the geodetic method are based on thickness changes within a certain time period. The glacier ice thickness change Δh is calculated as the pixel-wise difference of two digital elevation model (DEM) datasets acquired at t_i and t_{i+1}, respectively. The DEM raster datasets contain absolute altitude values (in m a. s. l.).

$$\Delta h_{t_i \rightarrow t_{i+1}} = DEM_{t_{i+1}} - DEM_{t_i} \quad . \tag{6}$$

The total volume change (ΔV) between the two dates is calculated by taking the elevation difference (Δh_k) at each pixel k and the DEM cell size (r), and summing these values across all K pixels within the glacier area at t_i (Zemp and others, 2013):

$$\Delta V = \sum_{i=k}^{K} \Delta h_k \cdot r^2 \quad . \tag{7}$$

To enable the comparison with the glaciological mass balance, the volume change (ΔV) must be expressed as specific mass balance (b_{geod}) in units of meters water equivalent (m w.e.) (Zemp and others, 2013). To account for changes in the glacier's extent over the observation period, it is necessary to divide the volume change by the mean glacier area (Florentine and others, 2023). The conversion is performed as follows:

$$b_{geod} = \frac{\Delta V}{\bar{S}} \cdot \frac{\bar{\rho}}{\rho_{water}} \quad , \tag{8}$$

where $\bar{S} = \frac{1}{2}(S_{t_i} + S_{t_{i+1}})$ is the mean glacier area between the initial (t_i) and final (t_{i+1}) observation dates. The term $\bar{\rho}/\rho_{water}$ is the ratio of the average bulk density of the glacier to the density of water (Zemp and others, 2013; Klug and others, 2018). Due to the near-complete loss of firn area at SSK (Cremona and others, 2026), a bulk density value of $\rho_{ice} = 900\,(\pm 2\,\%)$ kg m^{-3}, based on uncertainty estimates of ice density (Cogley, 2009), was used for volume-to-mass conversions for all annual geodetic datasets within the multi-method MB period.

The uncertainty of the geodetic mass balance is calculated following the comprehensive error propagation framework outlined by Zemp and others (2013). First, the uncertainty in the mean elevation change ($\sigma_{\overline{\Delta h}}$) is derived from the root mean square error (RMSE) of the elevation differences over stable, ice-free terrain, ensuring spatial autocorrelation is accounted for.

The uncertainty in the glacier area ($\sigma_{S_{t_i}}$) is estimated based on the spatial accuracy of the DEMs in the horizontal plane ($RMSE_{xy}$). Following standard buffer-based approaches for glacier outlines (e.g., Paul and others, 2013; Hugonnet and others, 2021), the area error is calculated by multiplying this linear error by the approximated perimeter of the glacier:

$$\sigma_{S_{t_i}} = P_{t_i} \cdot RMSE_{xy} \quad , \tag{9}$$

where P_{t_i} is the perimeter of the glacier at time t_i, approximated from the total area as $P_{t_i} \approx 2\sqrt{\pi S_{t_i}}$.

Assuming the uncertainties in the mean elevation change and the glacier area are independent, they are propagated into the total volume change uncertainty ($\sigma_{\Delta V}$) following Zemp and others (2013):

$$\sigma_{\Delta V} = \sqrt{(\sigma_{\overline{\Delta h}} S_{t_i})^2 + (\sigma_{S_{t_i}} \overline{\Delta h})^2} \quad , \tag{10}$$

where S_{t_i} is the total glacier surface area of the initial year, and $\overline{\Delta h}$ is the mean elevation change.

Finally, to convert this volumetric uncertainty into the uncertainty of the specific geodetic mass balance ($\sigma_{b_{geod}}$), the error associated with the volume-to-mass density conversion must be integrated. Following Zemp and others (2013), the geometric volume error ($\sigma_{\Delta V}$) and the density error (σ_ρ) are combined via root sum of squares:

$$\sigma_{b_{geod}} = \frac{1}{\bar{S} \cdot \rho_{water}} \sqrt{(\sigma_{\Delta V} \cdot \bar{\rho})^2 + (\Delta V \cdot \sigma_\rho)^2} \quad , \tag{11}$$

where $\bar{S}$ is the mean glacier area, $\bar{\rho}$ represents the average bulk density used for the conversion, and σ_ρ is the estimated uncertainty of that density assumption.

Table 1 lists the time periods for which geodetic mass balance values are available from SSK. In addition to the MB value published by Fischer (2011), we computed multi-year geodetic mass change for 2008 to 2023 and 2018 to 2025 using independent DEM datasets. Annual geodetic mass change for the years 2018 to 2025 is used for the main method-intercomparison.

2.3 Glacier area homogenisation and mass-balance intercomparison

2.3.1 Homogenisation and mass-balance intercomparison

To allow a meaningful comparison of mass-balance results obtained with fundamentally different methods, a homogenisation is considered necessary (Zemp and others, 2013). This study follows the framework for reanalysing mass-balance measurement series presented by Zemp and others (2013). Most crucially, the mass-balance results for all three methods were recalculated using the same glacier area, enabling a more insightful comparison of results without potential deviations related to discrepancies in glacier area resulting from different mapping approaches or underlying source data.

For the method intercomparison (2018–2025), all mass balance datasets (direct, semi-direct, geodetic) were homogenised using a common set of glacier outlines. These were digitised from orthophotos generated from annual UAV surveys.

Although data-acquisition timing varied slightly across years and methods (± 11 days to reference date on average), refer to Figure A1), these offsets remained within the 20-day window for which seasonal

Table 1. Geodetic mass balance datasets available for SSK. Dates are reported with the highest available temporal precision. For certain datasets, however, only the month or, respectively, the year of acquisition is known. The bulk density listed in this table was used for volume-to-mass conversions in the respective studies.

Acq. date t	Acq. date $t+1$	Data type	Bulk density (kg/m^3)	Data source/References
Long-term geodetic mass balance				
1969	1998	Refer to Groß (1988), Lambrecht and Kuhn (2007)	850	Fischer (2011)
2008-11	2023-09	Airborne LiDAR	900	Data: Land Salzburg (2025), analysis: this study
2018-09-21	2025-09-18	UAV-Photogrammetry	900	this study
Annual geodetic mass balance				
2018-09-21	2019-08-27	UAV-Photogrammetry	900	this study
2019-08-27	2020-09-15	UAV-Photogrammetry	900	this study
2020-09-15	2021-09-13	UAV-Photogrammetry	900	this study
2021-09-13	2022-09-13	UAV-Photogrammetry	900	this study
2022-09-13	2023-09-05	UAV-Photogrammetry	900	this study
2023-09-05	2024-09-11	UAV-Photogrammetry	900	this study
2024-09-11	2025-09-18	UAV-Photogrammetry	900	this study

effects on annual to multi-year balances were shown to be negligibly small (Hock and others, 2026). Hence, no additional temporal correction was applied during the MB homogenisation, consistent with common practice in geodetic intercomparison (Piermattei and others, 2024).

2.3.2 Assessing mapping uncertainty

During the intercomparison period, glacier outlines were manually mapped from satellite images or orthophotos by different analysts as part of their annual processing of the mass balance data. These outlines provide a baseline for estimating the mapping uncertainties related to different interpretations by the analysts. Depending on the year, two to three independently mapped outlines are available. It is important to note that these deviations in glacier surface area cannot be linked to the mass-balance method (see subsection 2.2), as the approach is the same for all methods, namely digitising the glacier outline based on the latest available orthophoto. We combined area deviations between outlines from the same year with the spatial agreement of the mapped glacier areas to estimate the uncertainty in total glacier area. The relative deviation of total mapped area between analysts, $\bar{\delta}_S$, is computed as the ratio of the standard

deviation of the individual mapped areas to their yearly mean, following, e.g., Conzelmann and others (2026):

$$\bar{\delta}_S = \frac{\sigma_S}{\bar{S}} \quad , \qquad \sigma_S = \sqrt{\frac{1}{N-1}\sum_{i=1}^{N}\left(S_i - \bar{S}\right)^2} \quad , \qquad \bar{S} = \frac{1}{N}\sum_{i=1}^{N} S_i \quad , \tag{12}$$

where S_i is the area mapped by analyst i and $\bar{S}$ the mean across all N outlines available for that year.

The spatial overlap of mapped glacier areas, commonly expressed as "Intersection over Union" (IoU), is calculated as follows:

$$IoU = \frac{\left|\bigcap_{i=1}^{N} S_i\right|}{\left|\bigcup_{i=1}^{N} S_i\right|} \quad , \tag{13}$$

i.e., IoU is the spatial agreement index for N analysts, calculated as the geometric intersection of all individual outlines divided by their total union. It quantifies mapping consensus by dividing the area where all N analysts agree by the total combined area mapped by any analyst. Consequently, the spatial disagreement rate would be expressed as $1 - IoU$.

Our combined metric for the glacier surface area uncertainty ϵ_S is:

$$\epsilon_S = \sqrt{(1 - IoU)^2 + (\bar{\delta}_S)^2} \quad , \tag{14}$$

Figure 4 illustrates the homogenised glacier surface change between 2018 and the latest observations from 2025, along with the corresponding relative deviations derived from the comparison of glacier outlines mapped by different analysts. Larger deviations among the methods under investigation are in the order of up to 0.08 km² (12 %). The inter-analyst deviation $\bar{\delta}_S$ is 3.6 %. The spatial overlap of mapped glacier outlines, as obtained using the IoU metric, is 0.91, indicating a degree of spatial misalignment.

As evident from Figure 4, there is no significant correlation between $\bar{\delta}_S$ and IoU, underlining the importance of taking both the scalar and spatial deviation into consideration to assess overall glacier outline mapping uncertainty. The combined mapping uncertainty ϵ_S, which integrates both scalar and spatial deviation (see Equation 14), amounts to 9.98 %. Note that the 12 % figure above is the *maximum* single-year scalar deviation, whereas ϵ_S (9.98 %) is the period-mean combined metric; the two are not directly comparable. The mean scalar deviation $\bar{\delta}_S$ is only 3.6 %, so most of ϵ_S derives from the spatial $(1 - IoU)$ term – which is exactly why a scalar metric alone understates mapping uncertainty.

Figure 5 shows the mapped glacier outlines obtained by three distinct analysts. Overall, the western ice margin – which corresponds to the highest-elevation section of the glacier – shows strong agreement. In

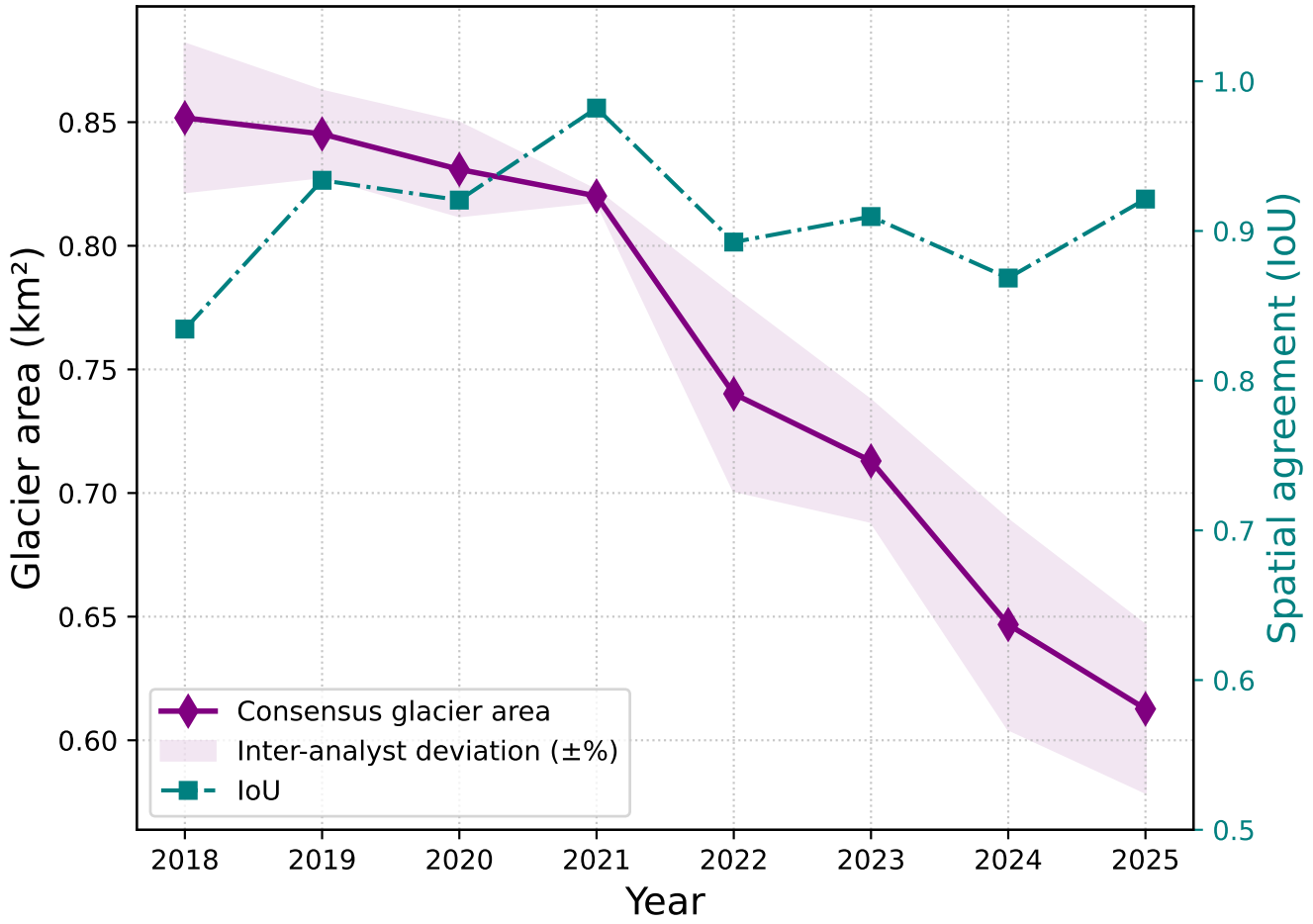

Fig. 4. Consensus glacier surface area for the period 2018–2025. The shaded envelope represents the inter-annual mean relative deviation in glacier area estimates among all analysts. The spatial correspondence between independently delineated glacier outlines is quantified using the IoU metric.

283 contrast, the northwestern part of the glacier is a key area of divergence. Additional inconsistencies between
284 analysts appear in the lower, eastern part of the glacier and around internal rock outcrops. From 2022
285 onward, when the glacier begins to fragment into three main sections, these differences become especially
286 apparent.

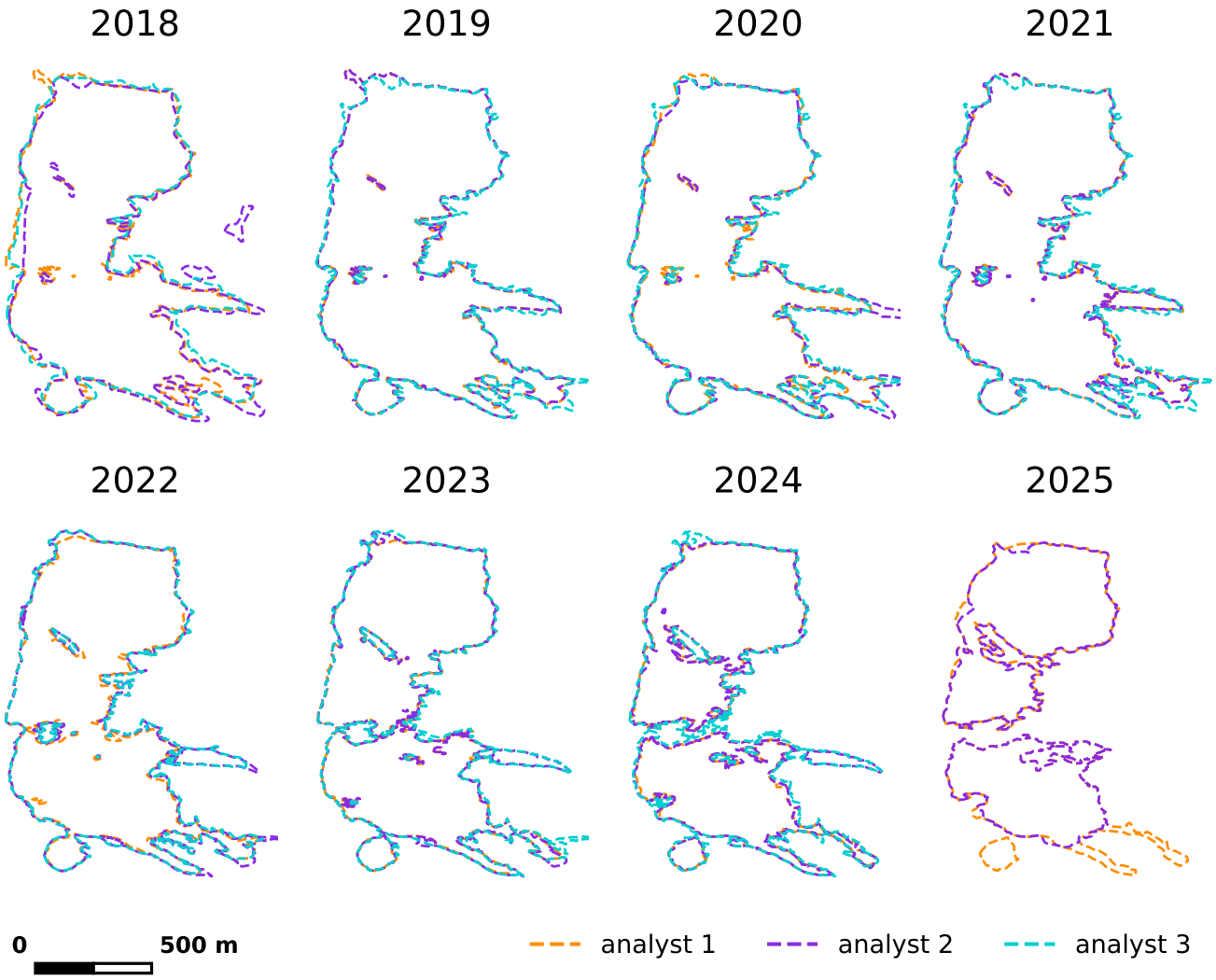

Fig. 5. Annual glacier extents from 2018 to 2025. Coloured outlines represent the digitisations of three different analysts. Note that for 2025, only two outlines were available.

287 *2.3.3 Mass-balance intercomparison*

288 The central question to be answered by the three-method intercomparison for the 2018–2025 period is
289 whether the results agree within the expected uncertainties of the respective methods. We approached this
290 by (i) directly comparing glacierwide annual results as well as spatial patterns in mass balance maps and

(ii) with an adapted version of the framework outlined in Zemp and others (2013) for determining whether systematic differences exist between methods. For (ii), we tested for systematic differences between the methods following Zemp and others (2013), comparing the cumulative mass change of the direct, semi-direct and geodetic methods pairwise over the intercomparison period. The 2018–2025 DEM difference serves as the reference geodetic balance, and is additionally tested against the cumulative sum of the annual geodetic epochs. The detailed test formulation, the propagation of period-of-record ("PoR") uncertainties, and the full set of input values are given in the Appendix (Table A3).

In addition to the annual comparisons for the 2018–2025 period, we provide an overview of longer-term mass balance comparisons for the time periods with available geodetic mass balance (Table 1). Intercomparison studies are essential for putting site-specific findings into a broader context. To this end, we present the method discrepancies observed at SSK alongside results from comparable studies.

3 RESULTS

3.1 Long-term mass-balance evaluation

3.1.1 Multi-annual mass-balance intercomparison at SSK

Comparing the cumulative (semi-) direct and geodetic mass balances between 1969 and 1998, Fischer (2011) reveals that the results differed by 4.7 m w.e. ($\Delta\, b$), or 0.16 m w.e. a^{-1}. ($\Delta\, b/n$). For the 15-year period of 2008–2015 (Table 1), we found a difference of 3 m w.e. (0.2 m w.e. a^{-1}) between the geodetic and the semi-direct method.

For the main intercomparison period (2018–2025), the geodetic mass balance computed from the 2018 and 2025 DEMs (referred to as b_{geo} in the following) is -10.97 m w.e. The cumulative sum of the annual geodetic mass balances for the same period is in good agreement with b_{geo} at -10.72 m w.e., i.e., an absolute difference of 0.25 m w.e. b_{geo} differs from the cumulative direct mass balance for the same period by 0.7 m w.e. (0.1 m w. a^{-1}), and from the cumulative semi-direct mass balance by $\Delta\, b = 1.78$ (0.25 m w.e. a^{-1}).

Hence, for 2018–2025, $\Delta\, b = 1.24$ averaged over all method combinations ($\Delta b/n = 0.18$ m w.e. a^{-1}). Averaging over all available periods (1969–1998, 2008–2015, 2018–2025) and methods, the mean annual absolute deviation is also 0.18 m w.e., which corresponds to a relative yearly deviation of 1.5 %. Table 2 provides details for all periods under investigation; a visualisation of the cumulative mass balances for all

three periods is shown in Figure 6.

Cumulating net mass changes over multiple years can mask potential fluctuations, as opposing changes may cancel each other out, leading to an underestimated deviation. Arguably, the mean absolute error (MAE) and the relative cumulated absolute difference per time step (mean absolute percentage error, $MAPE$) better reflect interannual variability. MAE and $MAPE$ can only be computed for the multi-method observation period with annual data (2018–2025) and result in:

$$MAE = 0.49 \text{ m w. e.} \quad , \quad MAPE = 36.36\ \%.$$

Table 2. Comparison of cumulative geodetic and (semi-) direct mass balances for the periods (a) 1969–1998, (b) 2008–2023, and (c) 2018–2025. Δb is calculated as the difference between the geodetic (b_{geo}) and the (semi-) direct MB, and divided by the number of years n covered by each period to obtain the yearly deviation.

Period	n	b_{geo} (m w.e.)	$b_{(semi-)dir}$ (m w.e.)	Δb (m w.e.)	$\Delta b/\lvert\bar{b}\rvert$ (%)	$\Delta b/n$ (m w.e. a^{-1})	References
(a) 1969–1998	29	−3.50	−8.18	4.68	57.21	0.16	Fischer (2011)
(b) 2008–2023	15	−15.48	−18.50	3.02	16.32	0.20	This study, source data: Land Salzburg (2025)
(c) 2018–2025 (dir)	7	−10.97	−11.67	0.70	6.00	0.10	This study
(c) 2018–2025 (semi)	7	−10.97	−13.61	2.64	21.48	0.37	This study

3.1.2 Test for systematic differences between methods

Following Zemp and others (2013), we tested whether the cumulative mass balances of any two methods differ significantly over the common period of record (2018–2025, $N = 7$). Refer to the Appendix (A.3) for details on the computation of the statistical test.

At the 95 % level the null hypothesis that two methods are equal is retained for every method pair: no two methods differ significantly (Table 3). The reduced discrepancy is smallest between the direct and geodetic methods ($\delta = -0.76$) and between the direct and semi-direct methods ($\delta = +1.08$), and largest for the semi-direct–geodetic comparison ($\delta = -1.68$). This last pair is the only one whose outcome depends on the confidence level: it is retained at 95 % but rejected at the more lenient 90 % level ($|\delta| > 1.645$), consistent with the growing divergence of the semi-direct method as its accumulation-area basis breaks down. The two full-period geodetic estimates – the cumulative sum of the annual epochs (−10.72 m w.e.) and the single 2018–2025 DEM difference (−10.97 m w.e.) – are statistically indistinguishable ($\delta = -0.60$), supporting the use of annual UAV differencing for multi-year change at this site (Klug and others, 2018). Substituting the

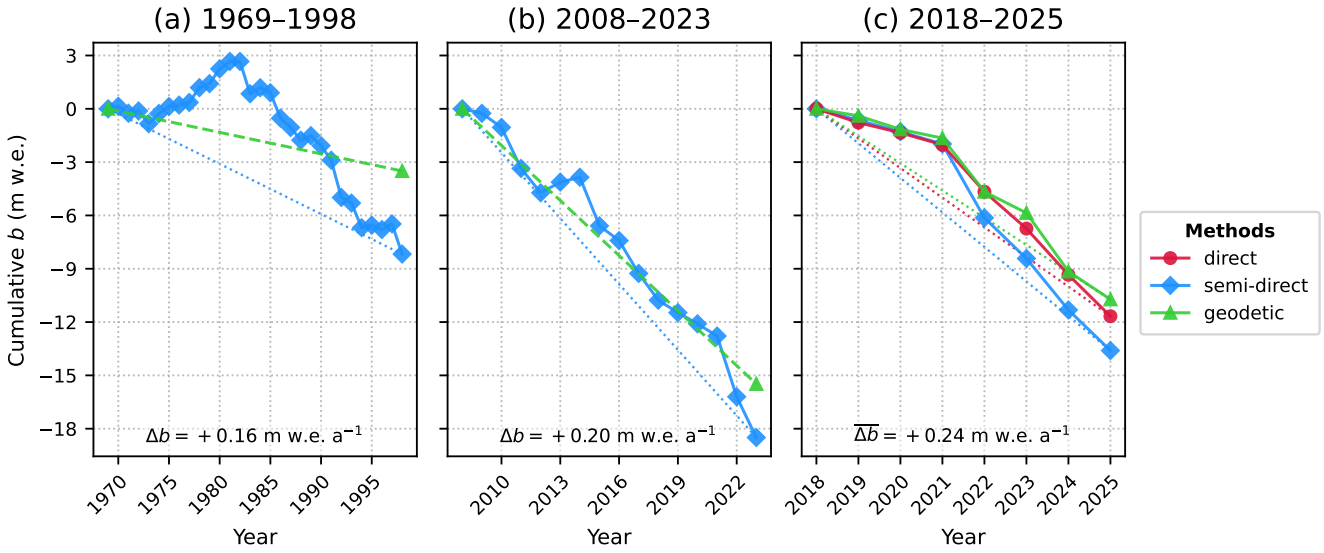

Fig. 6. Cumulative mass balances for the periods (a) 1969–1998, (b) 2008–2023, and (c) 2018–2025, comparing the (semi-) direct MB results with those obtained from the geodetic method. Note that (a) includes the calibration period of direct measurements. Dashed lines indicate interannual data acquisition periods; dotted lines indicate the cumulative MB for datasets with annual MB data available. Δb refers to the annual inter-method difference for periods (a) and (b); for period (c), $\overline{\Delta b}$ denotes the arithmetic mean of the two annual deviation values presented in Table 2.

annual-cumulative value for the DEM difference leaves every outcome unchanged (see Table A3). The high type-II error probabilities (β = 61–91 % at the 95 % level) reflect the short record and the comparatively large method uncertainties; "not significantly different" should therefore be read as "the data are consistent with agreement" rather than as proof of equality.

Table 3. Test for systematic differences between methods over 2018–2025 ($N = 7$), following Zemp and others (2013). Δ_{PoR} is the cumulative difference between the two methods, σ_{common} the combined uncertainty, δ the reduced discrepancy, H_0 the hypothesis that the two series are equal, and β the type-II error probability at $\alpha = 5\,\%$. The semi-direct–geodetic pair is the only one whose outcome differs between the 5 % and 10 % significance levels. An extended version (individual mass balances and uncertainties, β at both levels, and tests against the annual-cumulative geodetic value) is given in Table A3.

Method pair	Δ_{PoR} (m w.e.)	σ_{common} (m w.e.)	δ	H_0 (5 %)	H_0 (10 %)
Direct vs semi-direct	1.94	1.80	1.08	accepted	accepted
Direct vs geodetic (DEM)	−0.70	0.93	−0.76	accepted	accepted
Semi-direct vs geodetic (DEM)	−2.64	1.57	−1.68	accepted	**rejected**
Geodetic (DEM) vs geodetic (annual cum.)	−0.25	0.42	−0.60	accepted	accepted

3.1.3 Comparison with related research

Table A2 summarises key metrics from various historical and contemporary studies, providing a basis for comparison.

Since the semi-direct method was specifically developed for the SSK glacier, the comparison here is limited to the direct and geodetic methods. Figure 7a shows the correlation of cumulated b_{direct} and b_{geo} values, while Figure 7b illustrates the per-year correlation, emphasising the duration of the observation periods (n). With $\Delta b = 0.7$ m w. e., $\Delta b/|\bar{b}| = -3.09$ %, and the per-year deviation $\Delta b/n = 0.1$ m w. e. a^{-1}, the method intercomparison at SSK indicates good agreement (low method discrepancies) compared to other studies.

3.2 Annual mass balance

The specific mass balance in 2018 shows losses of -1.53±0.17 (semi-direct) and -1.90±0.34 m w.e. (direct). This is followed by three years of relatively moderate losses below 1 m w.e. From 2022 onwards, mass

balance is strongly negative in all years, with losses of more than 3 m w.e. depending on the method (Figure 8). The most negative value in the intercomparison period is the semi-direct specific mass balance for 2022 (-4.16±1.49 m w.e.). The direct method also indicates that 2022 (-2.64±0.34 m w.e.) is the most negative year, followed closely by 2024 (-2.60±0.34 m w.e.). The geodetic method shows slightly greater losses in 2024 than in 2022 (-3.30±0.13 m w.e. (2024), -3.02±0.13 m w.e. (2022)). For a complete overview of all mass balance values, see Table A1 in the Appendix.

The annual mass-balance results (see Figure 8) lie within method-specific uncertainties in 5 out of 8 years for all three methods. The direct and semi-direct methods yield mass-balance estimates that are mutually consistent within their respective uncertainty ranges for all years. By contrast, the mass-balance values derived from the direct and geodetic methods fall outside each other's uncertainty intervals in 3 of the 7 years considered, specifically in the three most recent years (2023–2025). The mass-balance estimates obtained from the semi-direct and geodetic methods lie outside one another's uncertainty ranges in 2 years (2023 and 2024).

In 2022, the MB value obtained from the semi-direct method is over 1 m w.e. more negative than the other two methods' results, yielding the largest deviation in absolute terms. However, as the uncertainty estimation for the semi-direct method scales with AAR and penalises very low AAR values (see Equation 5), the value is still considered within uncertainty for the three methods. The largest relative difference is the 2023 geodetic MB result, which is 48 % smaller than the semi-direct, and 43 % smaller than the direct value.

3.2.1 Spatially distributed mass balance

For the direct and the geodetic method, the MB intercomparison can be further examined in a spatial dimension. Figure 9 shows the annual MB results for both methods (a, b) and the associated spatial differences (c) as maps. As of 2022, the methods' MB results show remarkably different patterns, which is in line with greater absolute deviations visible in Figure 8.

The impression that the direct method generally records higher mass loss in the lower sections of the glacier is confirmed in Figure 10, which displays the cumulative mass balances of these two methods and their difference.

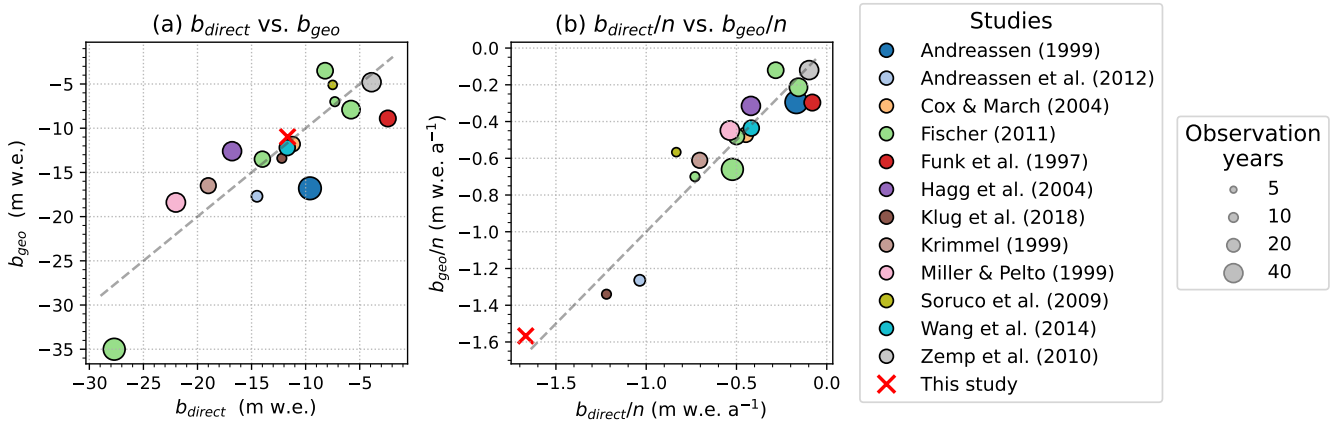

Fig. 7. Comparison with related mass-balance reanalysis or intercomparison studies. (a) shows the correlation of direct (b_{direct}) and geodetic (b_{geo}) mass balance; (b) shows the correlation of the per-year mass-balance values for b_{direct} and b_{geo}. This plot contains values listed in Table A2.

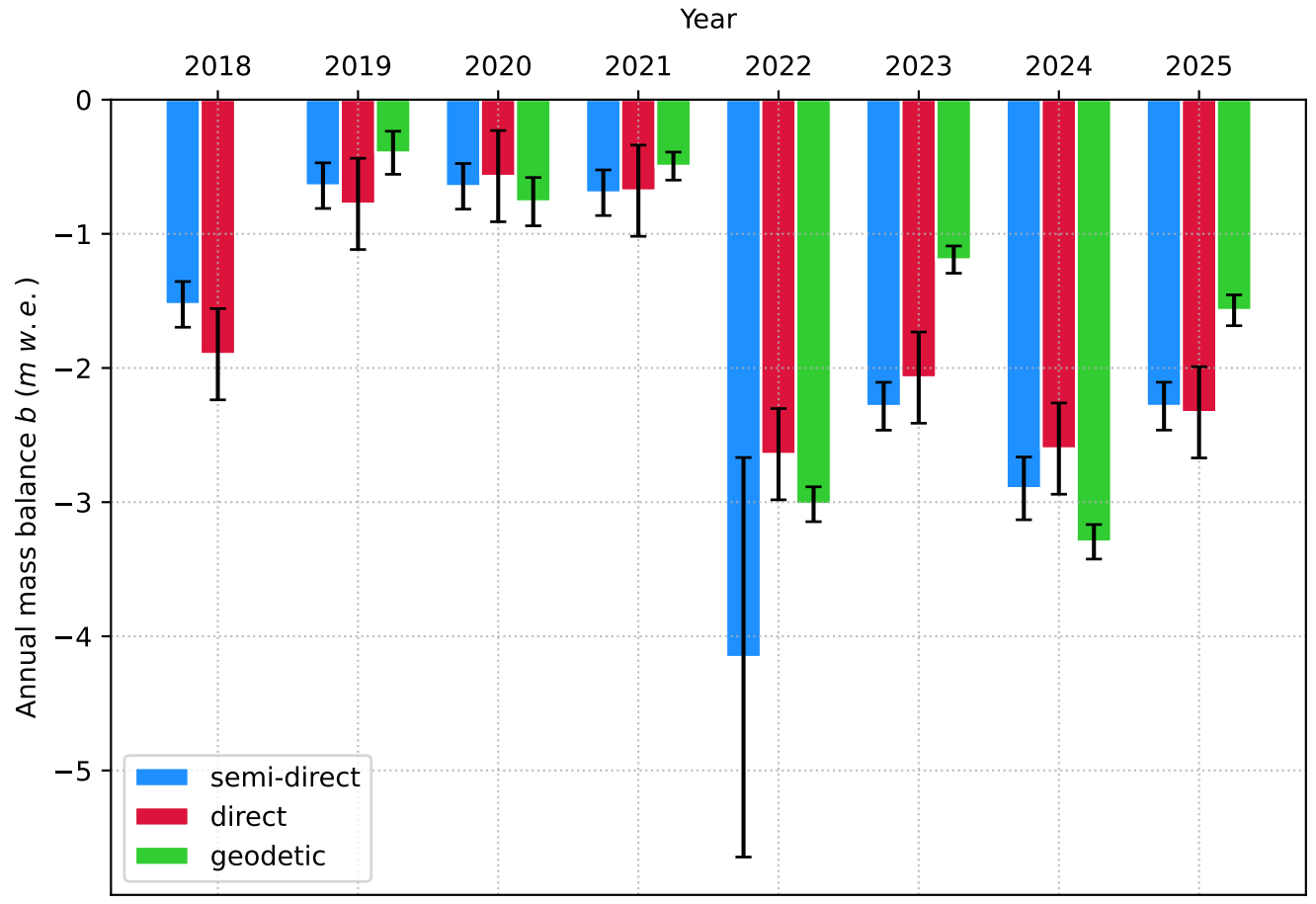

Fig. 8. Annual specific mass balance from 2018 to 2025 for the semi-direct, direct and geodetic method. The error bars indicate method-related uncertainties as defined per method in subsection 2.2. Note that geodetic MB observations are only available as of 2019.

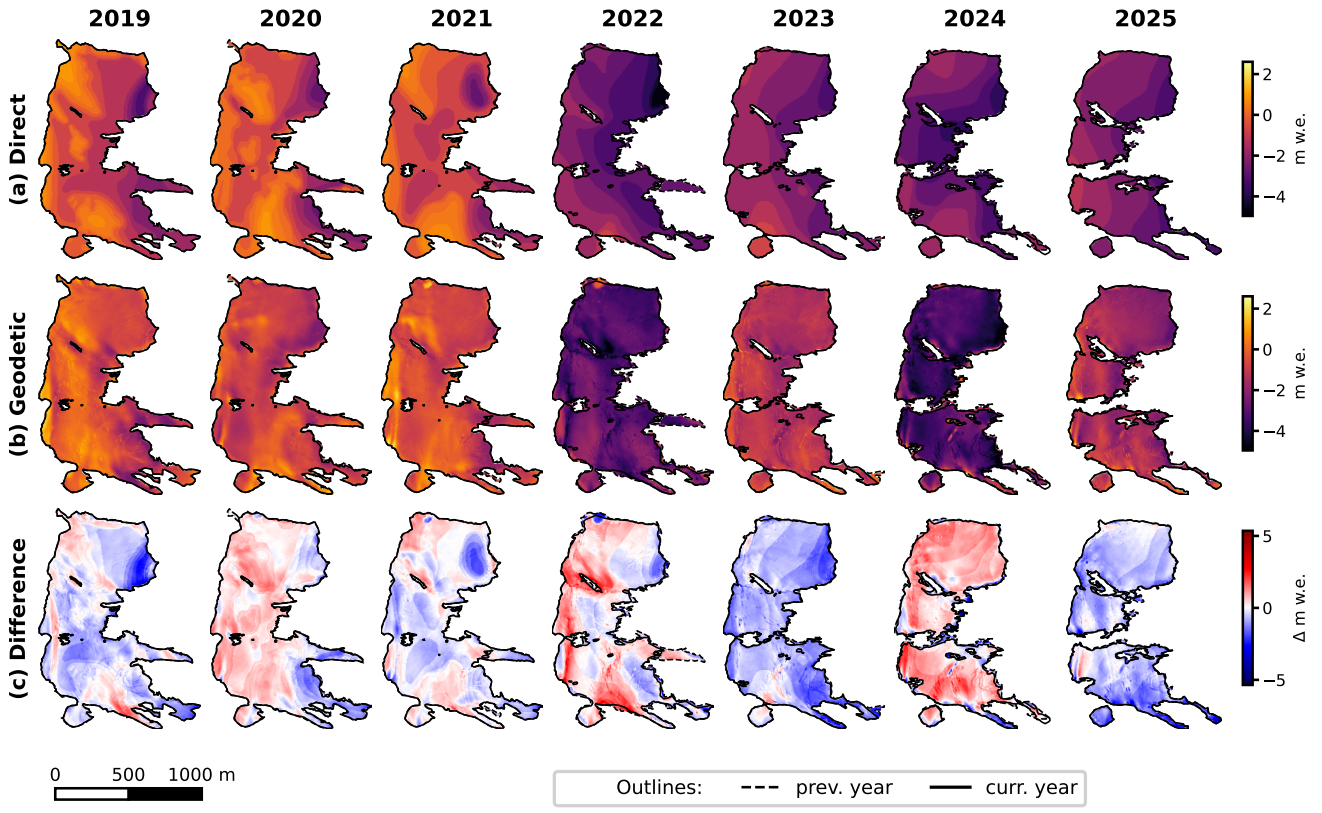

Fig. 9. Annual spatially distributed mass balance from 2019 to 2025 for (a) the direct and (b) the geodetic method. The difference between (a) and (b) is shown in the third plot (c). Note that these MB values were calculated using the previous year's glacier outline as the reference area.

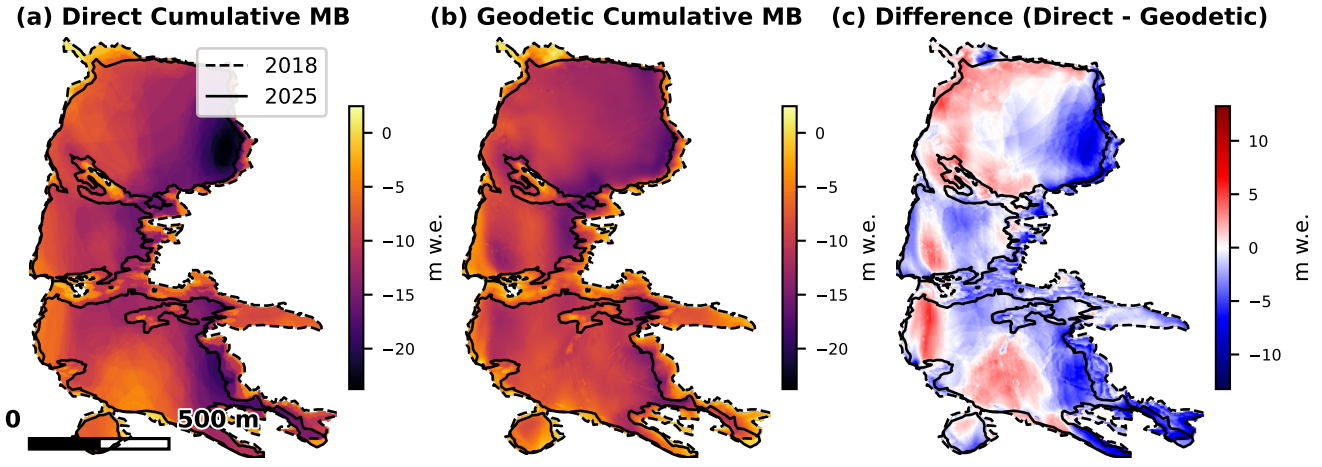

Fig. 10. Cumulative spatially distributed mass balance from 2019 to 2025 for (a) the direct and (b) the geodetic method. The difference between (a) and (b) is shown in the third plot (c).

3.2.2 Accumulation area agreement

The semi-direct method is primarily governed by the AAR and, hence, very sensitive to changes in the extent of the accumulation area. Figure 11 compares S_c as identified in the semi-direct method by mapping from imagery and S_c as obtained with the direct method and the contour line approach, as well as areas of positive elevation change as per the DEM-differencing.

The IoU (refer to Equation 13), visualised in yellow, indicates the accumulation area where all three methods agree. Despite the conceptual difference of the three methods, there is visible spatial alignment of areas of positive surface elevation gain, particularly in the first four years of this intercomparison exercise. Notably, the geodetic method also yields accumulation areas of positive surface elevation gain in the lower parts of the glacier

3.2.3 Direct vs semi-direct mass balance

As described in Sec. 2.2.2, the empirical relationships of the semi-direct method, i.e., the AAR governing the mass balance, were derived from a series of direct mass-balance measurements conducted between 1964 and 1980. The use of the logarithmic function in the MB calculations (see Equation 3 and Equation 2) makes the semi-direct method especially sensitive to the AAR, or the S_c value, respectively.

During this calibration period, the median AAR was 0.73, a value that has rarely been reached since and not at all during the multi-method observation period (2018–2025, Figure A2). AAR estimates from the semi-direct and direct methods also diverge markedly in several years, which may partly account for the discrepancies in the MB comparison (see Figure 8). This divergence becomes most pronounced from 2022 onward, when the direct method yields an AAR of 0, reflecting the glacier's transition to a state with little or no persistent accumulation area – a regime in which the semi-direct method's reliance on the AAR as a tuning parameter becomes problematic: once no accumulation area persists, the AAR loses its physical meaning as a predictor, and the semi-direct framework operates outside the range of conditions for which it was calibrated.

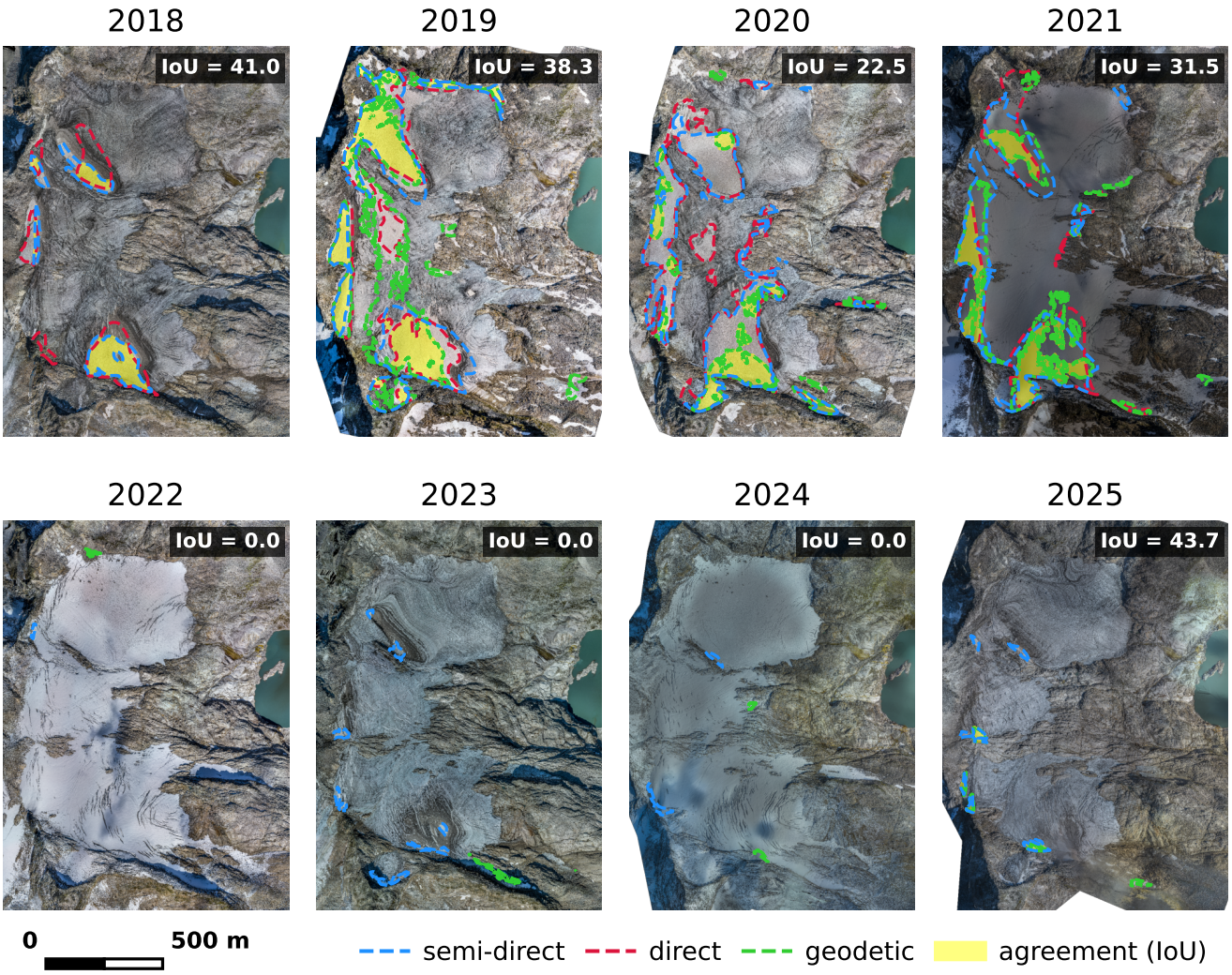

Fig. 11. Accumulation area as obtained with the direct, semi-direct, and geodetic method for the entire observation period (2018–2025). The yellow area indicates agreement across all methods, mathematically described by the IoU value. Note that no accumulation areas were observed from the direct method as of 2022 (IoU is only calculated for those methods with an $S_c > 0$).

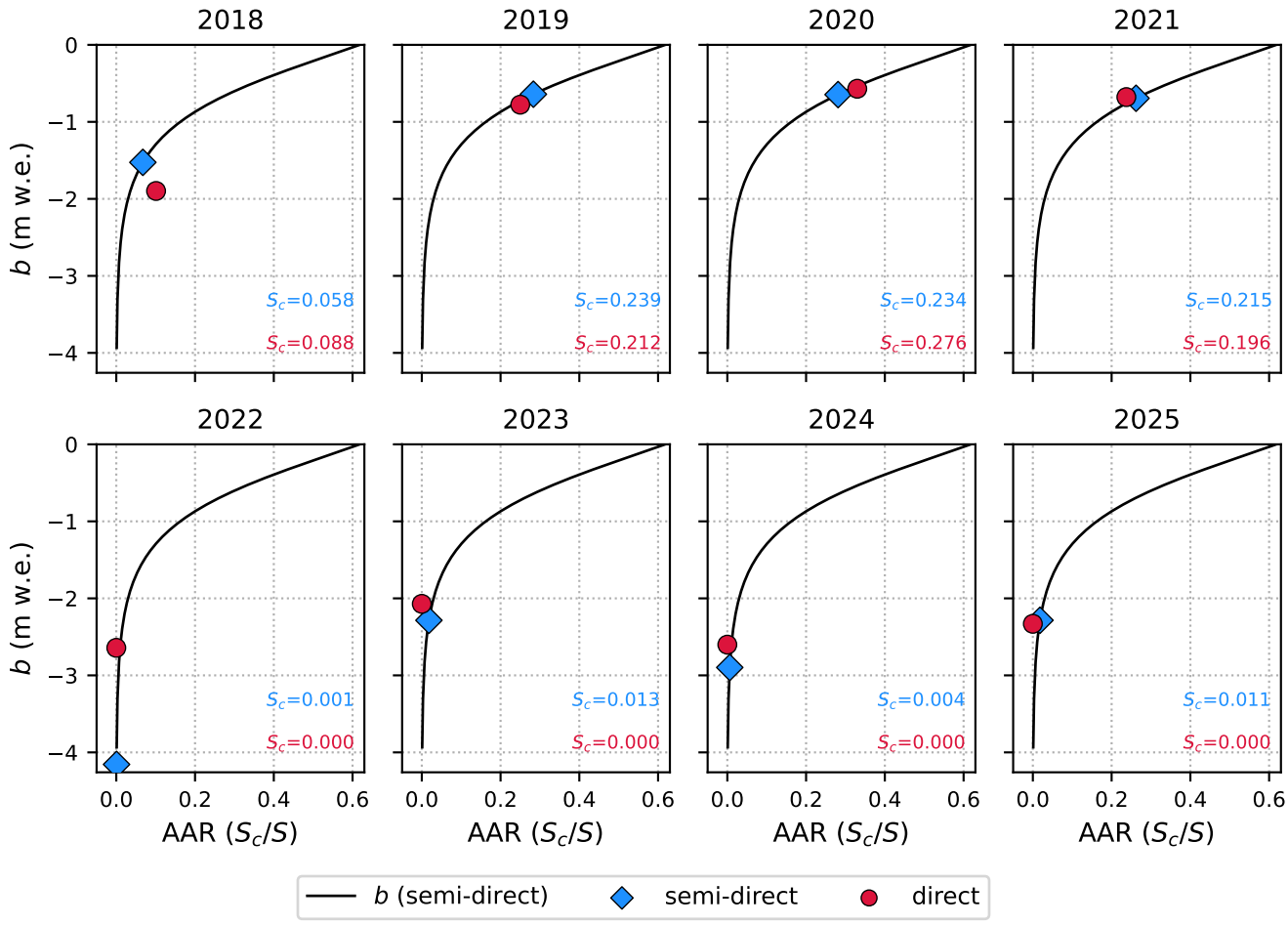

Fig. 12. The AAR is plotted against the net specific mass balance b for both the semi-direct and the direct method for each year of the multi-method monitoring period 2018–2025. The net mass balance for the semi-direct method is calculated using the equations described in subsubsection 2.2.2, and is therefore consistently plotted on the b-axis. The AAR and b values shown for the direct method are derived from in situ measurements. The net MB curve (black) indicates which b value the AAR of the direct method would correspond to if the semi-direct equations were applied.

4 DISCUSSION

4.1 From multi-annual to yearly mass-balance intercomparisons

At the multi-annual scale, the three methods behave largely as expected. The formal test for systematic differences (subsubsection 3.1.2, Table 3) retains the null hypothesis of equality for every method pair over 2018–2025: no two methods differ significantly at the 95 % level, the semi-direct–geodetic comparison being the closest to significance (and the only pair rejected at the more lenient 90 % level). This can be considered an early indication of the semi-direct method's growing divergence that we return to in subsubsection 4.2.2. The data are consistent with mutual agreement at the multi-annual scale, although the modest statistical power (β = 61–91 %, owing to the short record) means this is better stated as consistency-with-agreement than as proven equivalence. Contextualising these findings within the broader literature (Table A2, Figure 7) reveals that the agreement at SSK between the direct and geodetic methods – with a deviation of only 0.7 m w.e. over seven years ($\Delta b/n$ = 0.1 m w.e. a^{-1}) – is among the lowest reported in comparable studies.

However, cumulative metrics like Δb can mask interannual variability, as opposing deviations cancel out. The MAE (0.49 m w.e.) and MAPE (36.36 %) provide a more robust characterisation of year-to-year consistency and reveal annual scatter that is not captured by cumulative measures. We therefore recommend the complementary use of MAE and MAPE alongside Δb in future intercomparison exercises, as these metrics account for interannual variability regarding the magnitude of glacier volume change.

At higher temporal resolution, the picture is more complicated: All three methods yield MB results within their uncertainty ranges for most years of the intercomparison period 2018–2025, however, annual discrepancies are non-negligible: For example, the two most common methods', direct and geodetic, MB results are outside the above-mentioned uncertainty range for the last three consecutive years (2023–2025), which warrants further investigation.

Spatial analysis reveals patterns of disagreement that are not apparent in the scalar comparison alone. The direct method consistently records greater mass loss in the lower, fragmented sections of the glacier compared to the geodetic method (Figure 9, Figure 10). This may partially be explained by ice dynamics and is an expected pattern of divergence for the two methods. However, considering spatial divergence at annual scales, the discrepancies become more pronounced from 2022 onward, coinciding with the acceleration of glacier fragmentation. A possible explanation is that, as the glacier breaks into separate ice

bodies, (i) stake coverage thins over the fragments, degrading the direct method's interpolation, while (ii) the geodetic method may register debris redistribution rather than ice loss in the same low-elevation cells. The two effects act in opposite directions and so widen the apparent spatial divergence.

Historically, annual geodetic balances were considered too sensitive to short-term elevation noise, with multi-year DEM differencing regarded as more robust; Klug and others (2018) were among the first to show that annual differencing is reliable given sufficient data quality. Our results support this: the cumulative sum of the annual UAV epochs (−10.72 m w.e.) and the single 2018–2025 DEM difference (−10.97 m w.e.) agree to within 0.25 m w.e. and are statistically indistinguishable (see Sec. 3.1.2), indicating that high-resolution annual UAV surveys capture multi-year change without systematic drift at SSK.

4.2 Uncertainties, strengths and limitations

4.2.1 Mapping uncertainty and the need for homogenisation

Comparing the three datasets confirmed that outline homogenisation is necessary: inter-analyst differences in glacier surface area in the order of 10 %, driven not by mass-balance methodology but by the subjectivity of manual digitisation – particularly over debris cover, rock outcrops, and fragmented ice bodies, and compounded by differences in source imagery, sun angle, and shadowing (Linsbauer and others, 2021; Conzelmann and others, 2026; Hartl and others, 2026). Critically, we show that scalar deviations (δS_{rel}) do not adequately characterise mapping uncertainty when outlines diverge spatially while converging in total area. The Intersection over Union metric captures this spatial dimension and decorrelates from δS_{rel} (see Figure 4). We therefore recommend IoU as a standard complementary metric in glacier outline assessments, responding directly to the call by Hock and others (2026) for spatially resolved uncertainty information and complementing the homogenisation framework of Zemp and others (2013).

4.2.2 Method-inherent uncertainties, strengths and limitations

SSK has entered its terminal phase of recession, attaining a new system state in which boundary conditions differ fundamentally from those that prevailed when conventional methods for glacier mass-balance monitoring were originally developed. Consequently, the calibration parameters and underlying assumptions of all established methods are being increasingly challenged. **Direct method.** As the glacier surface continues to fragment, the representativeness of individual ablation stakes declines. Extrapolating point measurements across a disintegrating, topographically complex surface introduces interpolation errors that

are difficult to quantify with standard uncertainty frameworks (e.g., Thibert and Vincent, 2009; Zemp and others, 2013). Point-scale uncertainty frameworks such as that of Geibel and others (2022) – which explicitly account for stake placement biases and density assumptions – could be useful building blocks for future mass-balance assessments at SSK, although they do not by themselves address the spatial extrapolation to the glacier scale, which is a separate and increasingly important source of uncertainty at fragmenting glaciers. Furthermore, no accumulation area has been identified at SSK by direct measurements since 2022, indicating that the glacier has entered a phase of pure ablation.

Semi-direct method. The semi-direct approach belongs to the broader family of methods that infer glacier-wide balance from the accumulation-area ratio (AAR) the equilibrium-line altitude (ELA), or snow line metrics – empirical relationships calibrated against direct measurements that assume a quasi-stable link between the AAR/ELA and the net balance (Braithwaite, 1984; Rabatel and others, 2013). This assumption is increasingly untenable under rapid change: fixed accumulation-area ratios are now known to carry substantial, regime-dependent errors that grow as glaciers move away from equilibrium (Yang and others, 2026). At SSK, the relationships were derived during 1964–1980, when the median AAR was 0.73. This value has not been reached during the multi-method monitoring period (2018–2025), and since 2022, the direct method reports no accumulation area at all (AAR = 0). The logarithmic functions governing b_c and b_a (Equation 2, Equation 3) approach undefined limits as the AAR tends to zero, so the method now operates well outside its calibration range. While it still returns numerical outputs through 2025, the accumulation areas it infers from 2022 onward are inconsistent with direct observations (Figure A2), and the resulting balances carry highly uncertain physical meaning. This failure is not specific to SSK, but is inherent to AAR/ELA-based approaches once glaciers move into strong disequilibrium. A persistently low AAR – below roughly 30 % – signals the loss of a stable accumulation zone and a glacier in disequilibrium with climate (Pelto, 2010), precisely the regime in which the AAR–balance relationship loses its calibration basis. For small Alpine glaciers in particular, continued thinning drives the ELA towards or above the summit, so that the accumulation area shrinks to zero and even former high-elevation accumulation zones become firn-free (Carturan and others, 2020; Huss and Fischer, 2016; Hartl and others, 2025a). The semi-direct record at SSK is thus a concrete instance of a broader limitation: empirical relationships calibrated under near-equilibrium conditions cannot be assumed to extrapolate into regimes of severe disequilibrium, regardless of their historical performance.

Geodetic (UAV) method. The geodetic approach is technically advantageous for small, rapidly shrink-

ing glaciers because its relative uncertainty does not necessarily increase as the glacier area decreases. A well-known limitation of the geodetic method is that it records net surface-elevation change, and therefore cannot separate ice-mass loss from other surface processes such as debris accumulation, snowdrift, or supraglacial sediment redistribution (e.g., Fischer, 2011; Zemp and others, 2013). At SSK, this effect is particularly visible in the accumulation area comparison of Figure 11, where the geodetic method reports accumulation in areas coinciding with known debris accumulation (see Figure A3). This ambiguity requires careful interpretation, particularly as debris cover typically increases during glacier retreat. Independent tracking of debris thickness would help disentangle this signal.

Density estimates. For the conversion of ice thickness change to mass gain or loss, the geodetic method relies on density estimates, taken either from the literature (Cogley, 2009) or from parallel glaciological measurements. The geodetic volume-to-mass conversion relies on an assumed bulk density (here 900 kg m^{-3}). The associated uncertainty does not stem from variability in ice density itself – which is well constrained near 900 kg m^{-3} – but from not knowing what fraction of a given volume change is low-density snow or firn rather than ice. As SSK has lost essentially all of its firn zone, this ambiguity is now largely removed: the converted volume is almost entirely glacier ice, so the density-conversion uncertainty of the geodetic method is smaller in this terminal phase than for glaciers that still retain a substantial firn body. In this respect, late-stage retreat actually reduces this density-related uncertainty. We report mass balance in m w.e. for consistency with the multi-decadal SSK record, and note the recommendation of Hock and others (2026) to report mass change in units (e.g. kg m^{-2}) that permit unambiguous conversion between conventions for new datasets.

Data acquisition timing. Temporal offsets between measurement campaigns (Figure A1) are a further source of uncertainty common to all three methods. As noted in section 2, acquisition occurred within $\pm$11 days of the fixed reference date on average, i.e., well inside the $\sim$20-day window over which Hock and others (2026) found seasonal effects on annual to multi-year balances to be negligible. No temporal correction was therefore applied. However, this tolerance should not be read as the timing being unimportant: As SSK has been strongly negative since 2015, a given offset near the end of the ablation season translates into a larger mass-balance error than it would on a glacier closer to balance, since it is multiplied by a high ablation rate. This sensitivity motivates more frequent – ideally automated – acquisitions targeting the end of the ablation season as disintegration continues.

4.3 Implications for future MB monitoring and long-term MB record preservation

The long-term mass-balance series of SSK, extending back to 1949, constitutes one of the most valuable observational records in the Eastern Alps. The continuity of this record through method transitions – from direct measurement (1964–1980) through the semi-direct approach (1981–present) to the reinstatement of direct monitoring in 2017 and the addition of geodetic surveys from 2018 – is both its primary strength and its central methodological challenge. The long-term cumulative comparison (Table 2, Figure 6) indicates broadly consistent agreement between the geodetic and (semi-)direct methods across three independent comparison periods spanning more than five decades (1969–1998, 2008–2023, 2018–2025). As at the annual scale, however, the comparison is not strictly like-for-like — the historical periods rely on the semi-direct method alone, while the recent period also includes direct measurements — so the apparent stability of the multi-decadal offset cannot be firmly established from three heterogeneous periods. We present it as a pattern worth testing rather than an established systematic bias.

The direct and geodetic methods offer complementary strengths (spatial resolution for geodetic; process-specificity and seasonal resolution for direct), and their demonstrated agreement over 2018–2025 supports the feasibility of a joint record. However, the increasing spatial complexity of the fragmenting glacier poses challenges for both. Ultimately, the most robust approach for preserving the legacy record through SSK's final years is likely a combined geodetic-glaciological monitoring strategy to further examine potential method-related mismatches until SSK vanishes entirely. The homogenised, multi-method dataset published alongside this study provides a foundation for continued record-keeping.

Looking ahead and beyond SSK, late-stage Alpine glacier retreat requires an adaptive, multi-method monitoring strategy that captures both surface and subsurface processes. Importantly, monitoring programmes must be established on larger "successor" glaciers before terminal reference sites disappear to enable cross-calibration and data continuity (Huss and others, 2025; Linsbauer and others, 2025). High-resolution geodetic monitoring should be expanded beyond terminal glaciers to sites with long direct mass-balance series to enable cross-calibration across a wider range of climatic and geometric conditions. For rapidly changing glaciers such as SSK, more frequent (potentially automated) geodetic surveys would also improve attribution of short-term ablation signals.

Conventional surface-based monitoring and geodetic differencing provide only a superficial view of mass loss, failing to distinguish between surface melt and the increasingly significant contributions of internal and basal ablation (Fischer, 2011; Hösli and others, 2025). While geodetic surveys capture total volume

change, they cannot uniquely determine residual ice volume or quantify internal voids and subsurface melt processes (Ruols and others, 2025). Consequently, these surveys should be integrated with near-surface geophysical observations, such as Ground-Penetrating Radar (GPR), to accurately quantify remaining ice storage. This multi-method integration is essential to close the mass-balance budget and provide the high-resolution boundary conditions required to initialize and evaluate glacier evolution models through the terminal phase of retreat.

5 CONCLUSIONS

We compared three independent mass-balance methods – direct glaciological, semi-direct (AAR-based) and UAV-geodetic – at the disintegrating Stubacher Sonnblickkees over 2018–2025. We further embedded this intercomparison in a long-term context through geodetic–(semi-)direct comparisons spanning three independent periods back to 1969. No method pair differs significantly at the 95 % level during the 2018–2025 intercomparison period. The semi-direct–geodetic discrepancies are the closest to significance, an early indication of the semi-direct method's approaching breakdown, although the short record limits statistical power throughout. The annual deviation between the direct and geodetic methods (0.1 m w.e. a^{-1}) is among the lowest reported in comparable studies. The geodetic and (semi-)direct methods differ by a broadly similar amount across all three periods. This pattern warrants further investigation, but three heterogeneous periods are too few to establish it as a stable systematic offset. The cumulative sum of annual UAV-geodetic balances and the single 2018–2025 DEM differencing agree to within 0.25 m w.e. and are statistically indistinguishable. High-resolution annual geodetic surveys therefore capture multi-year mass change without systematic drift, and data quality is no longer the limiting factor for annual geodetic monitoring. At the annual scale, however, the methods show substantial year-to-year deviations that the multi-year agreement masks, a tension that becomes acute as disintegration accelerates.

At the same time, the final phase of retreat exposes each method's limits. The direct method remains the process-resolving backbone of the record but loses spatial representativeness as stake networks fragment with the glacier. The semi-direct method, calibrated for 1964–1980 conditions, now operates outside its empirical range: As the governing AAR reaches zero, the empirical relationships are no longer defined and the physical meaning of its output becomes increasingly uncertain. The geodetic method is comparatively robust to shrinkage, as its relative uncertainty does not necessarily grow with diminishing area and the density-conversion ambiguity diminishes with the loss of the firn body. None of the methods alone, however,

captures the full picture: independent methods remain mutually dependent for validation, and maintaining at least two in parallel is what allows method limits to be detected at all. For SSK's final years, the parallel continuation of the direct and geodetic programmes offers the most robust basis for extending the series.

Beyond SSK, the broader lesson is that late-stage glaciers must be monitored with parallel, complementary methods, and that such programmes need to be transferred to larger successor glaciers before terminal reference sites vanish, preserving continuity and cross-calibration. A further frontier is subsurface mass loss: because neither glaciological nor geodetic methods resolve internal and basal ablation, integrating near-surface geophysics such as GPR will be essential to close the mass-balance budget at disintegrating glaciers. Sustaining multi-method observations at sites in their terminal phase is what safeguards these records – and exposes the method limits no single approach can reveal – before the observational window closes for good.

Data availability All mass-balance data used in this study are available at the well-established data repository PANGAEA. The links in Table 4 take you directly to the websites where you can bulk-download the data:

Table 4. Overview of main and complementary datasets used in this study.

Dataset	Reference	URL
Direct (1964–1980) & semi-direct (1981–) MB	Slupetzky and others (2014)	https://doi.org/10.1594/PANGAEA.829950
Direct MB (2018–)	Gschwentner and others (2026)	https://doi.pangaea.de/10.1594/PANGAEA.993864
Geodetic MB (2019–)	Siebenbrunner (2026)	https://doi.pangaea.de/10.1594/PANGAEA.991024
Homogenised MB data series (2018–2025)	Siebenbrunner and others, in prep	
ALS data	Land Salzburg (2025)	https://www.salzburg.gv.at/themen/salzburg/sagis/sagis-downloadinfos
WGMS data	World Glacier Monitoring Service (2026)	https://doi.org/10.5904/WGMS-FOG-2026-02-10

Acknowledgments First and foremost, we thank Heinz Slupetzky and his team for their pioneering work at Stubacher Sonnblickkees for establishing the mass-balance monitoring programme in the 1960s. We further thank Hans Wiesenegger, former head of the Hydrological Service of Land Salzburg, for his enthusiasm to support the mass-balance efforts and for his commitment to reinitiate the direct mass balance in 2017, as well as his courage to test UAV-borne photogrammetry for mass-balance monitoring. Special

thanks are due to Barbara Staudinger (Hydrological Service of Land Salzburg) for her continued support of the monitoring programme and her valuable role in the preparation of this work. Finally, we thank everyone who helped with fieldwork at Stubacher Sonnblickkees for any of the methods throughout the years, and everyone who provided valuable feedback to improve this manuscript.

Author contributions **AG**: Data Curation, Writing Review & Editing; **ASi**: Conceptualisation, Methodology, Software, Validation, Formal analysis, Investigation, Data Curation, Writing - Original Draft, Writing Review & Editing, Visualisation; **ASo**: Data Curation, Writing Review & Editing; **BZ**: Investigation, Data Curation, Writing Review & Editing; **HW**: Resources, Data Curation, Writing Review & Editing, Project administration, Funding acquisition; **LH**: Software, Data Curation, Investigation, Supervision, Writing Review & Editing; **RD**: Data Curation, Writing Review & Editing.

Financial support All organisations involved in monitoring the mass balance at Stubacher Sonnblickkees received financial support from the Hydrological Service of Land Salzburg as well as the Federal Ministry of Agriculture and Forestry, Climate and Environmental Protection, Regions and Water Management. ASi acknowledges funding from the Austrian Research Promotion Agency (FFG), project MELT.AI, grant no. 61794780. LH acknowledges that this research was funded in whole or in part by the Austrian Science Fund (FWF) [10.55776/PAT2089925].

REFERENCES

Andreassen LM (1999) Comparing Traditional Mass Balance Measurements with Long-Term Volume Change Extracted from Topographical Maps: A Case Study of Storbreen Glacier in Jotunheimen, Norway, for the Period 1940-1997. *Geografiska Annaler. Series A, Physical Geography*, **81**(4), 467–476, ISSN 0435-3676

Andreassen LM, Nordli Ø, Rasmussen A, Melvold K and Nordli Ø (2012) Langfjordjøkelen, a rapidly shrinking glacier in northern Norway. *Journal of Glaciology*, **58**(209), 581–593, ISSN 0022-1430, 1727-5652 (doi:10.3189/2012JoG11J014)

Braithwaite RJ (1984) Can the Mass Balance of a Glacier be Estimated from its Equilibrium-Line Altitude? *Journal of Glaciology*, **30**(106), 364–368, ISSN 0022-1430, 1727-5652 (doi:10.3189/S0022143000006237)

Carturan L, Rastner P and Paul F (2020) On the disequilibrium response and climate change vulnerability of the mass-balance glaciers in the Alps. *Journal of Glaciology*, **66**(260), 1034–1050, ISSN 0022-1430, 1727-5652 (doi:10.1017/jog.2020.71)

628 Cogley JG (2009) Geodetic and direct mass-balance measurements: Comparison and joint analysis. *Annals of Glaciol-*
629 *ogy*, **50**(50), 96–100, ISSN 0260-3055, 1727-5644 (doi:10.3189/172756409787769744)

630 Cogley JG, Hock R, Rasmussen LA, Arendt AA, Bauder A, Braithwaite RJ, Jansson P, Kaser G, Möller M, Nicholson
631 L and Zemp M (2011) Glossary of glacier mass balance and related terms. Technical report, UNESCO/IHP, Paris

632 Conzelmann S, Seiser B, Fischer A, Lauria MV, Stocker-Waldhuber M, Bertolotti G and Hartl L (2026)
633 Mapping vanishing glaciers in Vorarlberg, Austria. *Annals of Glaciology*, 1–27, ISSN 0260-3055, 1727-5644
634 (doi:10.1017/aog.2026.10044)

635 Cox LH and March RS (2004) Comparison of geodetic and glaciological mass-balance techniques,
636 Gulkana Glacier, Alaska, U.S.A. *Journal of Glaciology*, **50**(170), 363–370, ISSN 0022-1430, 1727-5652
637 (doi:10.3189/172756504781829855)

638 Cremona A, Huss M, Landmann JM, Marty M, van der Meer M, Ginzler C and Farinotti D (2026) Seasonal mass
639 balance drivers for Swiss glaciers over 2010–2024 inferred from remote-sensing observations and modelling. *The*
640 *Cryosphere*, **20**(5), 3111–3130, ISSN 1994-0416 (doi:10.5194/tc-20-3111-2026)

641 Fischer A (2011) Comparison of direct and geodetic mass balances on a multi-annual time scale. *The Cryosphere*,
642 **5**(1), 107–124, ISSN 1994-0416 (doi:10.5194/tc-5-107-2011)

643 Fischer A, Seiser B, Stocker Waldhuber M, Mitterer C and Abermann J (2015) Tracing glacier changes in Austria from
644 the Little Ice Age to the present using a lidar-based high-resolution glacier inventory in Austria. *The Cryosphere*,
645 **9**(2), 753–766, ISSN 1994-0416 (doi:10.5194/tc-9-753-2015)

646 Florentine C, Sass L, McNeil C, Baker E and O'Neel S (2023) How to handle glacier area change in geodetic mass
647 balance. *Journal of Glaciology*, **69**(278), 2169–2175, ISSN 0022-1430, 1727-5652 (doi:10.1017/jog.2023.86)

648 Funk M, Morelli R and Stahel W (1997) Mass balance of Griesgletscher 1961-1994: Different methods of determina-
649 tion. *Zeitschrift für Gletscherkunde und Glazialgeologie*, **33**(1), 41–56, ISSN 0044-2836

650 Geibel L, Huss M, Kurzböck C, Hodel E, Bauder A and Farinotti D (2022) Rescue and homogenization of 140
651 years of glacier mass balance data in Switzerland. *Earth System Science Data*, **14**(7), 3293–3312, ISSN 1866-3508
652 (doi:10.5194/essd-14-3293-2022)

653 Geissler J, Mayer C, Jubanski J, Münzer U and Siegert F (2021) Analyzing glacier retreat and mass balances using
654 aerial and UAV photogrammetry in the Ötztal Alps, Austria. *The Cryosphere*, **15**(8), 3699–3717, ISSN 1994-0416
655 (doi:10.5194/tc-15-3699-2021)

656 Groß G (1988) Der Flächenverlust der Gletscher in Österreich 1850-1920-1969. *Der Flächenverlust der Gletscher in*
657 *Österreich 1850-1920-1969*, **23**(2), 131–141, ISSN 0044-2836

Gschwentner A, Bertolotti G, Seiser B, Hartl L, Stocker-Waldhuber M, Wiesenegger H and Fischer A (2026) Glacier mass balances and elevation zones of Stubacher Sonnblickkees from direct glaciological measurements, Hohe Tauern, Austria, 2017/2018 et seq

Günther R and Widlewski D (1986) Die Korrelation verschiedener Klimaelemente mit dem Massenhaushalt Alpiner und Skandinavischer Gletscher. *Zeitschrift für Gletscherkunde und Glazialgeologie*, **22**(2), 125–147

Hagg WJ, Braun LN, Uvarov VN and Makarevich KG (2004) A comparison of three methods of mass-balance determination in the Tuyuksu glacier region, Tien Shan, Central Asia. *Journal of Glaciology*, **50**(171), 505–510, ISSN 0022-1430, 1727-5652 (doi:10.3189/172756504781829783)

Hartl L, Seiser B, Stocker-Waldhuber M, Baldo A, Lauria MV and Fischer A (2024) Glaciological and meteorological monitoring at Long Term Ecological Research (LTER) sites Mullwitzkees and Venedigerkees, Austria, 2006–2022. *Earth System Science Data*, **16**(9), 4077–4101, ISSN 1866-3508 (doi:10.5194/essd-16-4077-2024)

Hartl L, Covi F, Stocker-Waldhuber M, Baldo A, Fugazza D, Di Mauro B and Naegeli K (2025a) Loss of accumulation zone exposes dark ice and drives increased ablation at Weißseespitze, Austria. *The Cryosphere*, **19**(8), 3329–3353, ISSN 1994-0416 (doi:10.5194/tc-19-3329-2025)

Hartl L, Schmitt P, Schuster L, Helfricht K, Abermann J and Maussion F (2025b) Recent observations and glacier modeling point towards near-complete glacier loss in western Austria (Ötztal and Stubai mountain range) if 1.5 °C is not met. *The Cryosphere*, **19**(3), 1431–1452, ISSN 1994-0416 (doi:10.5194/tc-19-1431-2025)

Hartl L, Abermann J, Akgün A, Bertolotti G, Bolch T, Conzelmann S, Diaconu CA, Hansche I, Hartig A, Haut A, Helfricht K, Hynek B, Kaucher MS, Kellerer-Pirklbauer A, Kogel AC, Krippes J, Lauria MV, Mayer C, Otto JC, Prinz R, Prölß S, Rieg L, Schönleber L, Schwaizer G, Seiser B, Stocker-Waldhuber M, Strudl M, Verhounik M and Zandler H (2026) On thin glacial ice: New Austrian Glacier Inventory shows accelerating glacier shrinkage and 31% area loss within two decades. *EGUsphere*, 1–39 (doi:10.5194/egusphere-2026-1241)

Hock R, Bliss A, Marzeion B, Giesen RH, Hirabayashi Y, Huss M, Radić V and Slangen ABA (2019) GlacierMIP – A model intercomparison of global-scale glacier mass-balance models and projections. *Journal of Glaciology*, **65**(251), 453–467, ISSN 0022-1430, 1727-5652 (doi:10.1017/jog.2019.22)

Hock R, Rasul C, Adler C, Cáceres B, Gruber S, Hirabayashi Y, Jackson M, Kääb A, Kang S, Kutuzov S, Milner Al, Molau U, Morin S, Orlove B and Steltzer H (2022) High Mountain Areas. In Intergovernmental Panel on Climate Change (IPCC) (ed.), *The Ocean and Cryosphere in a Changing Climate: Special Report of the Intergovernmental Panel on Climate Change*, 131–202, Cambridge University Press, Cambridge, ISBN 978-1-009-15796-4 (doi:10.1017/9781009157964.004)

688 Hock R, Huss M, Berthier E, Braun M, Gardner AS, Wouters B and Zemp M (2026) Toward improved comparability
689 of glacier mass-balance estimates: Challenges and recommendations. *Journal of Glaciology*, **72**, e49, ISSN 0022-
690 1430, 1727-5652 (doi:10.1017/jog.2026.10158)

691 Hoinkes H (1970) Methoden und Möglichkeiten von Massenhaushaltsstudien auf Gletschern. *Zeitschrift für*
692 *Gletscherkunde und Glazialgeologie*, **6**(1-2), 37–39

693 Hösli L, Ogier C, Bauder A, Huss M, Werder MA, Jacquemart M, Hodel E, Swift D, Cremona A, Walden J and
694 Farinotti D (2025) Subglacial cavity collapses on Swiss glaciers: Spatio-temporal distribution and mass loss con-
695 tribution. *Journal of Glaciology*, 1–35, ISSN 0022-1430, 1727-5652 (doi:10.1017/jog.2025.33)

696 Hugonnet R, McNabb R, Berthier E, Menounos B, Nuth C, Girod L, Farinotti D, Huss M, Dussaillant I, Brun F and
697 Kääb A (2021) Accelerated global glacier mass loss in the early twenty-first century. *Nature*, **592**(7856), 726–731,
698 ISSN 1476-4687 (doi:10.1038/s41586-021-03436-z)

699 Huss M and Fischer M (2016) Sensitivity of Very Small Glaciers in the Swiss Alps to Future Climate Change.
700 *Frontiers in Earth Science*, **4**, ISSN 2296-6463 (doi:10.3389/feart.2016.00034)

701 Huss M and Hock R (2018) Global-scale hydrological response to future glacier mass loss. *Nature Climate Change*,
702 **8**(2), 135–140, ISSN 1758-6798 (doi:10.1038/s41558-017-0049-x)

703 Huss M, Hock R, Bauder A and Funk M (2012) Conventional versus reference-surface mass balance. *Journal of*
704 *Glaciology*, **58**(208), 278–286, ISSN 0022-1430, 1727-5652 (doi:10.3189/2012JoG11J216)

705 Huss M, Bauder A, Linsbauer A, Gabbi J, Kappenberger G, Steinegger U and Farinotti D (2021) More than a century
706 of direct glacier mass-balance observations on Claridenfirn, Switzerland. *Journal of Glaciology*, **67**(264), 697–713,
707 ISSN 0022-1430, 1727-5652 (doi:10.1017/jog.2021.22)

708 Huss M, Fischer M, Linsbauer A and Bauder A (2025) Continuous monitoring of a glacier's extinction. *Annals of*
709 *Glaciology*, **66**, e27, ISSN 0260-3055, 1727-5644 (doi:10.1017/aog.2025.10024)

710 Klug C, Bollmann E, Galos SP, Nicholson L, Prinz R, Rieg L, Sailer R, Stötter J and Kaser G (2018) Geodetic
711 reanalysis of annual glaciological mass balances (2001–2011) of Hintereisferner, Austria. *The Cryosphere*, **12**(3),
712 833–849, ISSN 1994-0416 (doi:10.5194/tc-12-833-2018)

713 Krimmel R (1999) Analysis of difference between direct and geodetic mass balance measurements at South Cas-
714 cade Glacier, Washington. *Geografiska Annaler, Series A: Physical Geography*, **81**(4), 653–658 (doi:10.1111/1468-
715 0459.00093)

716 Kuhn M, Lambrecht A and Abermann J (2015) The Austrian glacier inventory GI 2, 1998, in ArcGIS (shapefile)
717 format (doi:10.1594/PANGAEA.844984)

718 Lambrecht A and Kuhn M (2007) Glacier changes in the Austrian Alps during the last three decades, de-
719 rived from the new Austrian glacier inventory. *Annals of Glaciology*, **46**, 177–184, ISSN 0260-3055, 1727-5644
720 (doi:10.3189/172756407782871341)

721 Land Salzburg (2025) ALS-Befliegungen

722 Landmann JM, Künsch HR, Huss M, Ogier C, Kalisch M and Farinotti D (2021) Assimilating near-real-time mass
723 balance stake readings into a model ensemble using a particle filter. *The Cryosphere*, **15**(11), 5017–5040, ISSN
724 1994-0416 (doi:10.5194/tc-15-5017-2021)

725 Linsbauer A, Huss M, Hodel E, Bauder A, Fischer M, Weidmann Y, Bärtschi H and Schmassmann E (2021) The New
726 Swiss Glacier Inventory SGI2016: From a Topographical to a Glaciological Dataset. *Frontiers in Earth Science*,
727 **9**, ISSN 2296-6463 (doi:10.3389/feart.2021.704189)

728 Linsbauer A, Huss M, Hodel E, Bauder A and Barandun M (2025) Vanished glaciers of the Swiss Alps: An
729 inventory-based assessment from 1973 to 2016. *Annals of Glaciology*, **66**, e33, ISSN 0260-3055, 1727-5644
730 (doi:10.1017/aog.2025.10031)

731 Miller MM and Pelto MS (1999) Mass Balance Measurements on the Lemon Creek Glacier, Juneau Icefield, Alaska
732 1953-1998. *Geografiska Annaler. Series A, Physical Geography*, **81**(4), 671–681, ISSN 04353676, 14680459

733 Østrem G, Brugman MM and Institute (Canada) NHR (1991) *Glacier Mass-balance Measurements: A Manual*
734 *for Field and Office Work*. National Hydrology Research Institute, Inland Waters Directorate, Conservation and
735 Protection, Environment Canada, ISBN 978-0-662-19000-4

736 Patzelt G (2015) The Austrian glacier inventory GI 1, 1969, in ArcGIS (shapefile) format
737 (doi:10.1594/PANGAEA.844983)

738 Paul F, Barrand NE, Baumann S, Berthier E, Bolch T, Casey K, Frey H, Joshi SP, Konovalov V, Bris RL, Mölg N,
739 Nosenko G, Nuth C, Pope A, Racoviteanu A, Rastner P, Raup B, Scharrer K, Steffen S and Winsvold S (2013)
740 On the accuracy of glacier outlines derived from remote-sensing data. *Annals of Glaciology*, **54**(63), 171–182, ISSN
741 0260-3055, 1727-5644 (doi:10.3189/2013AoG63A296)

742 Pelto MS (2010) Forecasting temperate alpine glacier survival from accumulation zone observations. *The Cryosphere*,
743 **4**(1), 67–75, ISSN 1994-0424 (doi:10.5194/tc-4-67-2010)

744 Piermattei L, Zemp M, Sommer C, Brun F, Braun MH, Andreassen LM, Belart JMC, Berthier E, Bhattacharya A,
745 Boehm Vock L, Bolch T, Dehecq A, Dussaillant I, Falaschi D, Florentine C, Floricioiu D, Ginzler C, Guillet G,
746 Hugonnet R, Huss M, Kääb A, King O, Klug C, Knuth F, Krieger L, La Frenierre J, McNabb R, McNeil C, Prinz
747 R, Sass L, Seehaus T, Shean D, Treichler D, Wendt A and Yang R (2024) Observing glacier elevation changes

from spaceborne optical and radar sensors – an inter-comparison experiment using ASTER and TanDEM-X data. *The Cryosphere*, **18**(7), 3195–3230, ISSN 1994-0416 (doi:10.5194/tc-18-3195-2024)

Rabatel A, Letréguilly A, Dedieu JP and Eckert N (2013) Changes in glacier equilibrium-line altitude in the western Alps from 1984 to 2010: Evaluation by remote sensing and modeling of the morpho-topographic and climate controls. *The Cryosphere*, **7**(5), 1455–1471, ISSN 1994-0424 (doi:10.5194/tc-7-1455-2013)

Ruols B, Klahold J, Farinotti D and Irving J (2025) 4D GPR imaging of a near-terminus glacier collapse feature. *The Cryosphere*, **19**(9), 4045–4059, ISSN 1994-0416 (doi:10.5194/tc-19-4045-2025)

Siebenbrunner A (2026) Geodetic glacier mass balances of Stubacher Sonnblickkees, Hohe Tauern Range, Eastern Alps, Austria, 2019 et seq (doi:10.1594/PANGAEA.991024)

Slupetzky H (1989) The mass balance series of the Stubaier Sonnblickkees 1958/59 to1987/88. *Zeitschrift für Gletscherkunde und Glazialgeologie*, **25**(1), 69–89, ISSN 0044-2836

Slupetzky H (2015) Die Massenbilanzreihe vom Stubacher Sonnblickkees 1946 bis 2014 und die semidirekte Berechnung des Massenhaushalts von Gletschern. *Zeitschrift für Gletscherkunde und Glazialgeologie*, 167–200

Slupetzky H, Ehgartner G and Zagel B (2014) Glacier mass balances of Stubacher Sonnblickkees, Hohe Tauern Range, Eastern Alps, Austria, 1958/1959 et seq (doi:10.1594/PANGAEA.829950)

Soruco A, Vincent C, Francou B, Ribstein P, Berger T, Sicart JE, Wagnon P, Arnaud Y, Favier V and Lejeune Y (2009) Mass balance of Glaciar Zongo, Bolivia, between 1956 and 2006, using glaciological, hydrological and geodetic methods. *Annals of Glaciology*, **50**(50), 1–8, ISSN 0260-3055, 1727-5644 (doi:10.3189/172756409787769799)

Thibert E and Vincent C (2009) Best possible estimation of mass balance combining glaciological and geodetic methods. *Annals of Glaciology*, **50**(50), 112–118, ISSN 0260-3055, 1727-5644 (doi:10.3189/172756409787769546)

Van Tricht L, Huybrechts P, Van Breedam J, Vanhulle A, Van Oost K and Zekollari H (2021) Estimating surface mass balance patterns from unoccupied aerial vehicle measurements in the ablation area of the Morteratsch–Pers glacier complex (Switzerland). *The Cryosphere*, **15**(9), 4445–4464, ISSN 1994-0416 (doi:10.5194/tc-15-4445-2021)

Van Tricht L, Zekollari H, Huss M, Rounce DR, Schuster L, Aguayo R, Schmitt P, Maussion F, Tober B and Farinotti D (2025) Peak glacier extinction in the mid-twenty-first century. *Nature Climate Change*, 1–5, ISSN 1758-6798 (doi:10.1038/s41558-025-02513-9)

Wang P, Li Z, Li H, Wang W and Yao H (2014) Comparison of glaciological and geodetic mass balance at Urumqi Glacier No. 1, Tian Shan, Central Asia. *Global and Planetary Change*, **114**, 14–22, ISSN 0921-8181 (doi:10.1016/j.gloplacha.2014.01.001)

Westoby MJ, Brasington J, Glasser NF, Hambrey MJ and Reynolds JM (2012) 'Structure-from-Motion' photogrammetry: A low-cost, effective tool for geoscience applications. *Geomorphology*, **179**, 300–314, ISSN 0169-555X (doi:10.1016/j.geomorph.2012.08.021)

World Glacier Monitoring Service (2026) Fluctuations of Glaciers (FoG) Database (doi:10.5904/WGMS-FOG-2026-02-10)

Yang W, Mackintosh AN, Cooper EL, Li Y, Jones RS, Chu W and Tielidze LG (2026) Global estimates of glacier equilibrium-line altitude ratios for enhanced paleoclimate reconstructions. *Communications Earth & Environment*, **7**(1), 391, ISSN 2662-4435 (doi:10.1038/s43247-026-03391-5)

Zagel B, Wiesenegger H, Junker RR and Ehgartner G (2024) Comprehensive Overview of Long-Term Ecosystem Research Datasets at LTER Site Oberes Stubachtal. *Data*, **9**(10), 110, ISSN 2306-5729 (doi:10.3390/data9100110)

Zemp M, Jansson P, Holmlund P, Gärtner-Roer I, Koblet T, Thee P and Haeberli W (2010) Reanalysis of multi-temporal aerial images of Storglaciären, Sweden (1959-99) - Part 2: Comparison of glaciological and volumetric mass balances. *The Cryosphere*, **4**(3), 345–357, ISSN 1994-0416 (doi:10.5194/tc-4-345-2010)

Zemp M, Thibert E, Huss M, Stumm D, Rolstad Denby C, Nuth C, Nussbaumer SU, Moholdt G, Mercer A, Mayer C, Joerg PC, Jansson P, Hynek B, Fischer A, Escher-Vetter H, Elvehøy H and Andreassen LM (2013) Reanalysing glacier mass balance measurement series. *The Cryosphere*, **7**(4), 1227–1245, ISSN 1994-0416 (doi:10.5194/tc-7-1227-2013)

Zemp M, Jakob L, Dussaillant I, Nussbaumer SU, Gourmelen N, Dubber S, A G, Abdullahi S, Andreassen LM, Berthier E, Bhattacharya A, Blazquez A, Boehm Vock LF, Bolch T, Box J, Braun MH, Brun F, Cicero E, Colgan W, Eckert N, Farinotti D, Florentine C, Floricioiu D, Gardner A, Harig C, Hassan J, Hugonnet R, Huss M, Jóhannesson T, Liang CCA, Ke CQ, Khan SA, King O, Kneib M, Krieger L, Maussion F, Mattea E, McNabb R, Menounos B, Miles E, Moholdt G, Nilsson J, Pálsson F, Pfeffer J, Piermattei L, Plummer S, Richter A, Sasgen I, Schuster L, Seehaus T, Shen X, Sommer C, Sutterley T, Treichler D, Velicogna I, Wouters B, Zekollari H, Zheng W and The GlaMBIE Team (2025) Community estimate of global glacier mass changes from 2000 to 2023. *Nature*, **639**(8054), 382–388, ISSN 1476-4687 (doi:10.1038/s41586-024-08545-z)

A APPENDIX

A.1 Timing of data acquisition

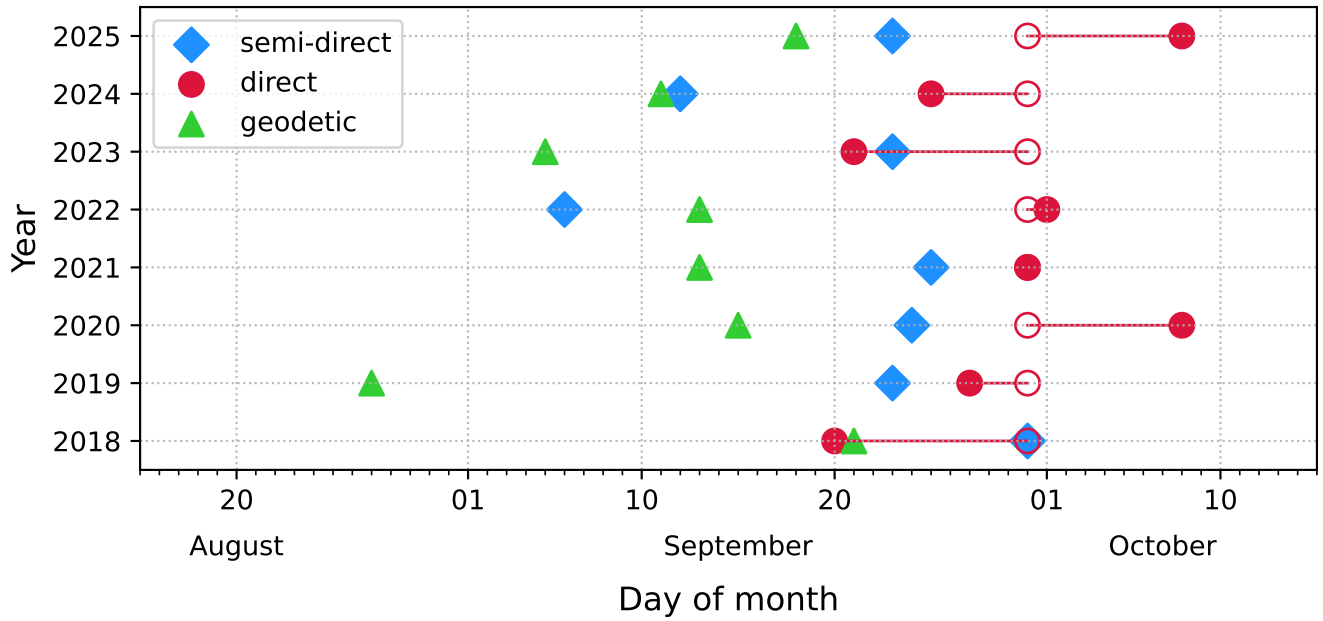

Fig. A1. Timing of data acquisition for the annual mass balance for all datasets from 2018 to 2025. The field measurements obtained with the direct method were adjusted to the hydrological year (indicated by unfilled markers).

A.2 Mass-balance results for all three methods (2018–2025)

Table A1. Annual homogenised glacier area S and mass-balance estimates b with associated uncertainties for the intercomparison period 2018–2025. Geodetic balances are unavailable for 2018; the elevated 2022 semi-direct uncertainty reflects the AAR-based error term at very low accumulation-area ratios (see Equation 5). Refer to Figure 8 for a visualisation of the mass-balance values.

Year	S (km^2)	b (m w.e.)		
		direct	semi-direct	geodetic
2018	0.85	-1.90±0.34	-1.53±0.17	
2019	0.85	-0.78±0.34	-0.64±0.17	-0.40±0.16
2020	0.83	-0.57±0.34	-0.65±0.17	-0.76±0.18
2021	0.82	-0.68±0.34	-0.69±0.17	-0.50±0.10
2022	0.74	-2.64±0.34	-4.16±1.49	-3.02±0.13
2023	0.71	-2.07±0.34	-2.29±0.18	-1.19±0.10
2024	0.65	-2.60±0.34	-2.90±0.23	-3.30±0.13
2025	0.61	-2.33±0.34	-2.28±0.18	-1.57±0.11

A.2.1 Accumulation area ratio over time

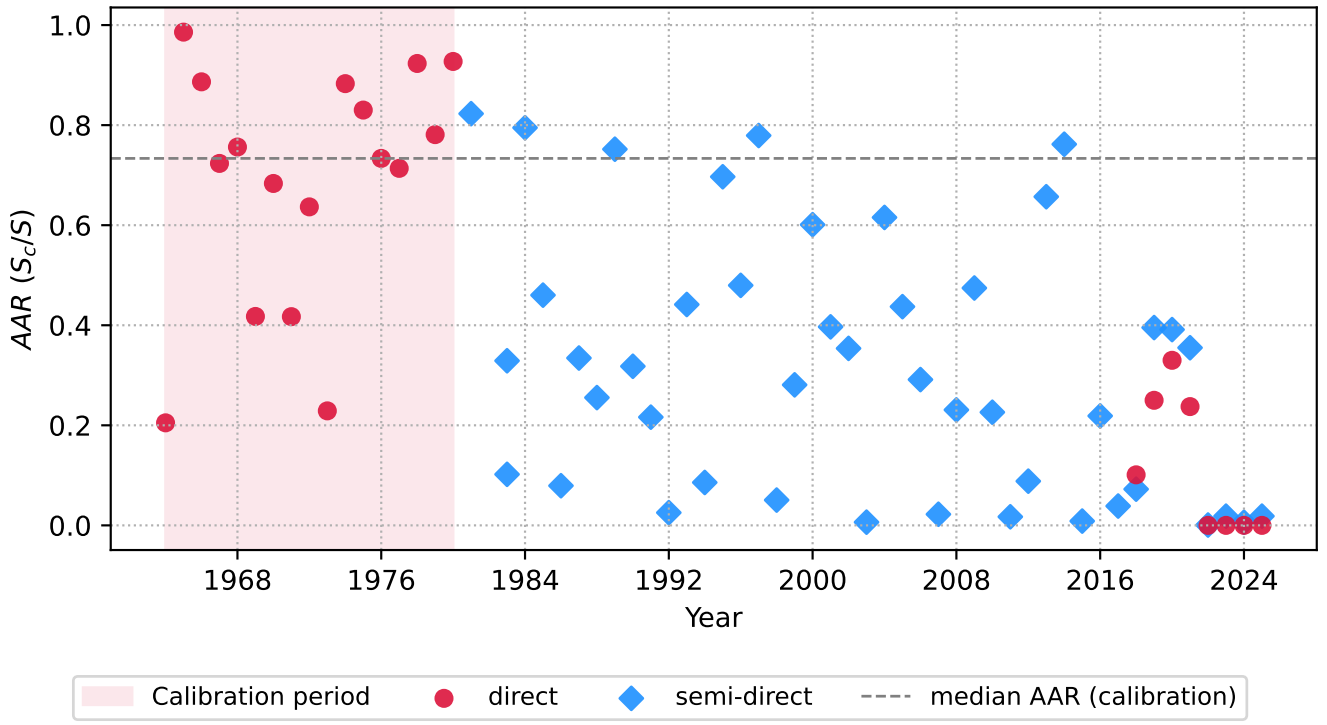

Fig. A2. Development of the accumulation area ratio (AAR) over time. The dashed line indicates the median AAR value during the calibration period (1964–1980) (Slupetzky and others, 2014).

806 ### *A.2.2 Related MB intercomparison studies*

Table A2. Comparative metrics from related mass-balance intercomparison studies (in alphabetical order). b_{geo} and b_{direct} are the geodetic and glaciological mass balance, respectively. Δb is the difference between b_{geo} and b_{direct} ($\Delta b = b_{geo} - b_{direct}$). The number of years covered by the observation period is denoted as n. The per-year-deviation is given as $\Delta b/n$. The relative difference between b_{geo} and b_{direct} is given as $\Delta b/|\bar{b}|$, where $|\bar{b}|$ is the absolute value of the mean of b_{geo} and b_{direct}.

Study	Glacier(s)	b_{geo}	b_{direct}	$\Delta b/\lvert\bar{b}\rvert$	Δb	n	$\Delta b/n$
		(m w. e.)	(m w. e.)	%	(m w. e.)		(m w. e. a^{-1})
Andreassen (1999)	Storbreen (SB)	−16.80	−9.60	−27.27	−7.20	57	−0.13
Andreassen and others (2012)	Langfjordjøkelen (LJ)	−17.70	−14.50	−9.94	−3.20	14	−0.23
Cox and March (2004)	Gulkana Glacier (GU)	−11.80	−11.20	−2.61	−0.60	25	−0.02
Fischer (2011)	Hintereisferner (HEF)	−35.00	−27.70	−11.64	−7.30	53	−0.14
Fischer (2011)	Jamtalferner (JAM)	−7.00	−7.30	2.10	0.30	10	0.03
Fischer (2011)	Kesselwandferner (KWF)	−7.90	−5.80	−15.33	−2.10	37	−0.06
Fischer (2011)	SSK	−3.50	−8.20	40.17	4.70	29	0.16
Fischer (2011)	Vernagtferner (VF)	−13.50	−14.00	1.82	0.50	28	0.02
Funk and others (1997)	Griesgletscher (GG)	−8.90	−2.40	−57.52	−6.50	30	−0.22
Hagg and others (2004)	Central Tuyusku Glacier (CTG)	−12.60	−16.80	14.29	4.20	40	0.11
Klug and others (2018)	Hintereisferner (HEF)	−13.40	−12.20	−4.69	−1.20	10	−0.12
Krimmel (1999)	South Cascade (SC)	−16.50	−19.00	7.04	2.50	27	0.09
Miller and Pelto (1999)	Lemon Creek (LC)	−18.40	−22.00	8.91	3.60	41	0.09
Zemp and others (2010)	Storglaciären (SG)	−4.80	−3.90	−10.34	−0.90	40	−0.02
Soruco and others (2009)	Zongo Glacier (ZG)	−5.10	−7.50	19.05	2.40	9	0.27
Wang and others (2014)	Urumqi Glacier (UG)	−12.20	−11.70	−2.09	−0.50	28	−0.02
This study	SSK (2018–2025)	−10.97	−11.67	3.09	0.70	7	0.10

* b_{direct} was calculated from b_{geo} using $\rho = 850$ kg m^{-3}, according to Fischer (2011).

A.3 Hypothesis test for systematic differences between methods

For each method pair, the cumulative discrepancy over the period of record (2018–2025, $N = 7$), $\Delta_{\mathrm{PoR}} = B_1 - B_2$, was normalised by the combined uncertainty $\sigma_{\mathrm{common}} = \sqrt{\sigma_1^2 + \sigma_2^2}$ to give the reduced discrepancy $\delta = \Delta_{\mathrm{PoR}}/\sigma_{\mathrm{common}}$ (Eqs. 19–21 in Zemp and others, 2013). The null hypothesis that the two series are equal is retained where $|\delta| \leqslant 1.96$ (95 %) and $|\delta| \leqslant 1.645$ (90 %); the corresponding type-II error probability β (Eq. 24 therein) is reported at both levels. Period-of-record uncertainties were propagated from the annual values in Table A1: the direct method from the uniform $\sigma_b = 0.34$ m w.e. a^{-1}; the semi-direct method and the annual-cumulative geodetic balance as the quadratic sum of their annual uncertainties; and the 2018–2025 geodetic DEM difference through the error-propagation chain described in Sec. 2.2.3, which for this firn-free survey is dominated by the density-conversion term ($\sigma_{\mathrm{geod}} \approx 0.22$ m w.e.). Internal and basal balance corrections were assumed negligible at this small glacier. As the reference geodetic balance for the comparisons with the direct and semi-direct methods, we use the DEM difference; the annual-cumulative estimate is tested against it for consistency and used to confirm that the outcomes are insensitive to this choice (lower block of Table A3).

Table A3. Extended results of the test for systematic differences between methods (2018–2025, $N = 7$), following Zemp and others (2013). B_1, B_2 are the cumulative period-of-record balances of the two series and σ_1, σ_2 their propagated uncertainties; $\Delta_{\mathrm{PoR}} = B_1 - B_2$, $\sigma_{\mathrm{common}} = \sqrt{\sigma_1^2 + \sigma_2^2}$, $\delta = \Delta_{\mathrm{PoR}}/\sigma_{\mathrm{common}}$. H_0 (equality of the two series) and the type-II error probability β are reported at both the 5 % and 10 % significance levels. The lower block repeats the surface-method comparisons against the annual-cumulative geodetic balance instead of the DEM difference.

Method pair	B_1	σ_1	B_2	σ_2	Δ_{PoR}	σ_{c}	δ	H_0^5	β^5	H_0^{10}	β^{10}
	(m w.e.)								(%)		(%)
Direct vs semi-direct	−11.67	0.90	−13.61	1.56	1.94	1.80	1.08	accepted	81	accepted	71
Direct vs geodetic (DEM)	−11.67	0.90	−10.97	0.22	−0.70	0.93	−0.76	accepted	88	accepted	80
Semi-direct vs geodetic (DEM)	−13.61	1.56	−10.97	0.22	−2.64	1.57	−1.68	accepted	61	rejected	49
Geodetic (DEM) vs geod. (cum.)	−10.97	0.22	−10.72	0.35	−0.25	0.42	−0.60	accepted	91	accepted	84
Direct vs geodetic (cum.)	−11.67	0.90	−10.72	0.35	−0.95	0.97	−0.98	accepted	83	accepted	74
Semi-direct vs geodetic (cum.)	−13.61	1.56	−10.72	0.35	−2.89	1.60	−1.81	accepted	56	rejected	43

A.4 Misclassified debris accumulation

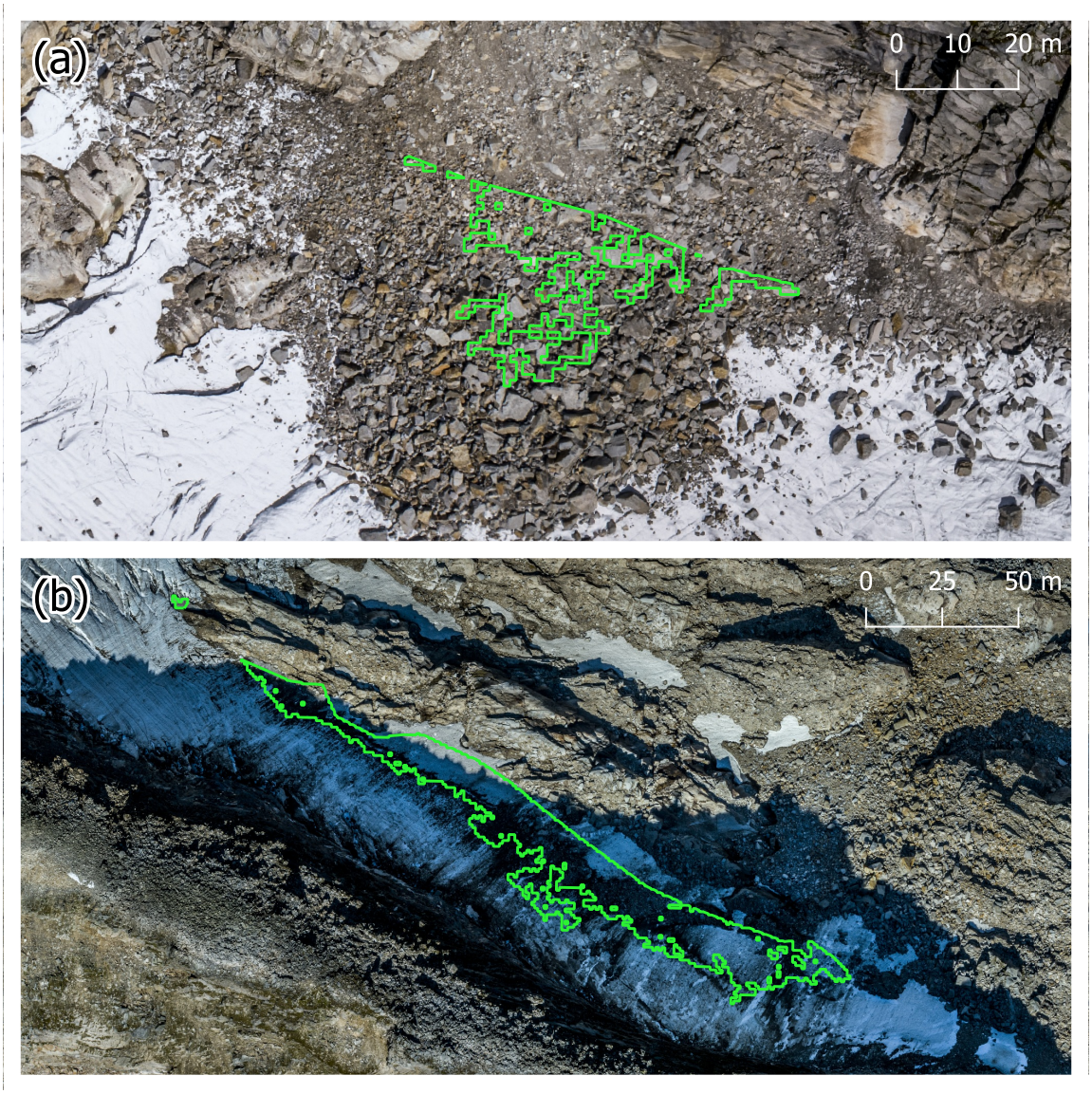

Fig. A3. Supraglacial debris accumulation in areas where the geodetic method records positive surface-elevation change (green polygons), shown for (a) 2022 and (b) 2023. Such debris cover can raise the surface without a corresponding gain in ice mass, so these localised elevation gains may be misinterpreted as accumulation, illustrating why elevation-based signals require careful interpretation (see Figure 11).